Title

Firing of *Streptomyces coelicolor* contractile injection system requires the membrane protein CisA

Authors

Bastien Casu[1], Joseph W. Sallmen[2], Peter E. Haas[1], Pavel Afanasyev[1], Jingwei Xu[1], Susan Schlimpert[2, *], Martin Pilhofer[1, *]

Affiliations

[1]Department of Biology, Institute of Molecular Biology & Biophysics, Eidgenössische Technische Hochschule Zürich, Otto-Stern-Weg 5, 8093 Zürich, Switzerland

[2]John Innes Center, Department of Molecular Microbiology, Norwich Research Park, Norwich, NR4 7UH, United Kingdom

Contact Info

* Correspondence: Susan.Schlimpert@jic.ac.uk (S.S.) and pilhofer@biol.ethz.ch (M.P.)

Abstract

Bacterial contractile injection systems (CIS) are phage tail-like macromolecular complexes that mediate cell-cell interactions by injecting effector proteins into target cells. CIS^{Sc} from *Streptomyces coelicolor* are distinct because they induce regulated cell death under stress, impacting the organism's life cycle. It remains unknown whether CIS^{Sc} require accessory proteins to function.

Here we characterize the putative membrane adaptor CisA, a conserved factor in CIS^{Sc} gene clusters across *Streptomyces* species. We show by cryo-electron tomography imaging and *in vivo* assays that CIS^{Sc} contraction and function depend on CisA. Using single-particle cryo-electron microscopy, we provide an atomic model of the extended CIS^{Sc} apparatus; however, CisA is not part of the complex. Instead, our findings show that CisA is a membrane protein with a cytoplasmic N-terminus predicted to interact with CIS^{Sc} components, thereby providing a possible mechanism for mediating CIS^{Sc} recruitment to the membrane and subsequent firing.

Our work shows that CIS function in multicellular bacteria is distinct from Type 6 Secretion Systems and extracellular CIS, and possibly evolved due to the role of CIS^{Sc} in regulated cell death.

Keywords: bacterial development/cellular microbiology/contractile phage tail/ghost cells/multicellularity

37 # Introduction

38 Bacteria employ different types of contractile injection systems (CIS) to mediate cell-cell
39 interactions or to function in regulated cell death[1]. CIS are evolutionarily and structurally
40 related to contractile tails of bacteriophages and are comprised of core modules including a
41 baseplate, a contractile sheath, and an inner tube [2,3]. CIS firing is triggered by a conformational
42 change within the baseplate[4,5] and results in the contraction of the sheath, which in turn propels
43 the inner tube along with the spike tip. Tube expulsion facilitates the release of associated
44 effector proteins into target cells or into the extracellular space[6,7].

45 Bioinformatic analyses have shown that CIS are conserved across diverse microbial phyla,
46 including Gram-negative and Gram-positive bacteria, as well as archaea[8,9]. Based on their
47 distinct modes of action, CIS can be categorized into two main groups: intracellular type VI
48 secretion systems (T6SS) and extracellular CIS (eCIS). T6SS are abundant among Gram-
49 negative bacteria and in some archaea, and they are anchored to the cytoplasmic membrane
50 during assembly and firing[10–12]. A crucial component of the T6SS is the baseplate, which acts
51 as a nucleus for T6SS assembly and mediates the binding of the T6SS particles to the
52 cytoplasmic membrane until contraction. Upon contraction, the spike and inner tube are
53 propelled out of the cell and into an adjacent cell or into the medium. eCIS, on the other hand,
54 are assembled as free-floating particles in the cytoplasm and are subsequently released into the
55 extracellular space upon lysis of the producer cell [13–16]. Following the release, eCIS attach to
56 the surface of target cells via their tail fibers, followed by contraction and puncturing of the
57 target cell envelope.

58 Besides T6SS and eCIS, there is accumulating evidence of additional CIS assemblies with
59 distinct modes of action in bacteria. For example, in multicellular cyanobacteria, CIS are
60 anchored to the intracellular thylakoid membrane stacks via an extension of the baseplate
61 components and have been proposed to function in cell lysis and the formation of "ghost cells"
62 in response to stress conditions[17]. Furthermore, several recent studies reported the production
63 of free-floating cytoplasmic CIS particles in the multicellular Gram-positive *Streptomyces*
64 bacteria, affecting cellular development through presumably slightly different mechanisms[18–
65 22].

66 *Streptomyces* are best known for producing a plethora of medically and industrially important
67 secondary metabolites, including molecules with antimicrobial, antifungal, anticancer or
68 immunosuppressive properties. The production of these molecules is tightly coordinated with
69 the *Streptomyces* developmental life cycle that encompasses two filamentous cell types,
70 including vegetative hyphae that grow by tip extension and branching to scavenge for nutrients,
71 as well as reproductive (aerial) hyphae that eventually differentiate into chains of spores. These
72 spores can then be dispersed to restart the life cycle[23,24]. Using *Streptomyces coelicolor* as a
73 model, we and others previously demonstrated that *S. coelicolor* CIS (CIS^{Sc}) mediate a form
74 of regulated cell death in response to exogenous stress and are also activated by unknown
75 cellular signals, thereby impacting the timing of sporulation and secondary metabolite
76 production (Figure 1a)[18,19].

77 It remains unclear whether CIS^{Sc} contraction occurs while the CIS^{Sc} particles are free-floating
78 in the cytoplasm or whether this is dependent on an interaction with the membrane. Moreover,
79 CIS encoded in *Streptomyces* genomes lack clear homologs for tail fiber components or a T6SS
80 trans-envelope complex, raising the question of how CIS^{Sc} particles could potentially interact
81 with the cytoplasmic membrane. We recently noted an uncharacterized protein[18,19], SCO4242,
82 that is encoded just downstream of the baseplate components in the CIS^{Sc} gene cluster, a
83 location that usually encodes tail fibers from conventional eCIS[13,16,25]. Importantly, SCO4242
84 is widely conserved in *Streptomyces cis* gene clusters[18,19]. We will therefore refer to the gene
85 product of SCO4242 as CisA for "CIS^{Sc}-associated protein A." Here we set out to assess the
86 importance of CisA for CIS^{Sc} function and its putative role as a membrane anchor.

87 # Results and Discussion

88 ## CisA is required for CIS^{Sc} contraction *in situ*

89 To explore the role of CisA (SCO4242) in CIS^{Sc} contraction and function, we first generated
90 an *S. coelicolor* Δ*cisA* null mutant. Negative stain electron microscopy (EM) imaging of CIS^{Sc}
91 particles that were purified from Δ*cisA* mutant cells showed assemblies in the contracted
92 conformation, similar to the CIS particles purified from the wildtype (WT) (Fig. 1b/c). We then
93 imaged vegetative hyphae of the WT, the Δ*cisA* mutant and the complemented mutant
94 (Δ*cisA/cisA*$^{+}$) by cryo-electron tomography (cryoET) (270 tomograms in total, n=3
95 experiments). The observed CIS^{Sc} particles in intact hyphae of these three imaged strains did
96 not reveal discernable differences, indicating that CisA is not required for CIS^{Sc} assembly. As
97 observed previously, we detected three states of cellular integrity of *Streptomyces* hyphae,
98 including 'intact hyphae', 'partially lysed hyphae' and 'ghost cells' (EV1a-c)[18]. Importantly,
99 *cisA*-deficient hyphae only contained CIS^{Sc} particles in the extended conformation irrespective
100 of the cellular integrity (Fig. 1e, EV1a-d). This is in stark contrast to 'ghost cells' derived from
101 hyphae of the WT and the Δ*cisA/cisA*$^{+}$ complementation strain, in which CIS^{Sc} particles were
102 predominantly found in the contracted conformation (Fig. 1d/f). These results indicate that
103 CisA is required for the contraction of CIS^{Sc} *in situ*.

104 ## CryoEM structure of the extended CIS^{Sc} assembly

105 The CIS^{Sc} gene cluster consists of 19 predicted open reading frames (accessions *SCO4242-*
106 *4260*) (Fig. 2a), including genes with sequence similarities to potential CIS structural
107 components (*cis1-cis16*), as well as additional genes with unknown functions (including
108 *cisA*)[18,19]. To determine whether CisA is an integral component of CIS^{Sc}, we set out to elucidate
109 the high-resolution structure of purified CIS^{Sc} particles from a non-contractile CIS^{Sc} mutant[18].
110 The purified assemblies were then subjected to single particle cryo-electron microscopy
111 (cryoEM) for structure determination (EV2), yielding the first high-resolution model of the
112 CIS^{Sc} in its extended conformation, which also presents the first example of a CIS IId subtype[8].

113 Our model showed that extended CIS^{Sc} particles share the conserved CIS architecture,
114 including three modules: cap, sheath-tube and baseplate (Fig. 2b). We processed the dataset
115 using an established workflow that was previously employed to produce the atomic model for

116 other CIS (EV2)[13,17]. The resulting maps of the baseplate and the cap reached resolutions of
117 3.5 and 3.4 Å, respectively. The quality of the final maps from the two modules enabled *de*
118 *novo* structural modelling (EV3, Table EV1). The model was further refined by integrating
119 symmetry-related protein subunits into a complete model of the entire CIS^{Sc} (Fig. 2b).

120 The final model of CIS^{Sc} comprised 783 polypeptide chains that assemble into a bullet-shaped
121 particle measuring 268 nm in length (Fig. 2b/c). The distal end of the CIS^{Sc} is capped by a tail
122 terminator complex (Fig. 2c/e). This cap comprises one protein, Cis16, forming a C6-
123 symmetrical complex that terminates the inner tube and sheath, respectively. This minimal
124 architecture resembles the cap complexes of PVC or Pyocin R2 CISs, but it is different from
125 the more complex AlgoCIS from *A. machipongonensis* and AFP from *S. entomophila*
126 (EV4)[13,16,25,26]. The structures of the CIS^{Sc} sheath-tube module have been discussed
127 previously[18]. Here we found that the module consists of 61 sheath layers (Cis2-L_1–L_{61}) and 60
128 tube layers (Cis1-L_1-L_{60}) (Fig. 2b/d).

129 The baseplate module consists of a heteromeric assembly of the proteins Cis1b/7/8/9/11/12
130 (Fig. 2b/c). The symmetry transition from the inner tube (Cis1a, C6) to the VgrG-like spike
131 (Cis8, C3) is adapted by two layers of the tube initiators Cis1b and Cis7. The first layer of the
132 sheath (Cis2) is bound to the conserved gp25-like protein Cis9, which connects to the baseplate
133 'wedges' composed of Cis11 and Cis12 (Fig. 2b/c). Importantly, the CIS^{Sc} 'wedges' consist of
134 two copies of Cis11 and one copy of Cis12 (Fig. 2f), resembling the baseplate of Pyocin R2[26].
135 This is in contrast to other previously reported eCIS, whose baseplate wedge comprises only
136 one Cis11/12 component (AlgoCIS, AFP, PVC) and a Cis11 extension forming a cage around
137 the spike (AlgoCIS) (EV4)[13,16,25].

138 Out of the 19 predicted open reading frames in the CIS^{Sc} gene cluster (Fig. 2a), nine encoded
139 proteins were present in the final reconstruction, all with atomic models built (Fig. 2b/c).
140 However, we did not detect a density for CisA in our model, suggesting that CisA is not part
141 of purified CIS^{Sc} particles but may interact via a different mechanism. This is consistent with
142 mass spectrometry results that indicate the absence of CisA peptides from purified CIS^{Sc}
143 particles (Fig. 2a)[18]. We speculate that a CIS^{Sc}-CisA interaction may not be preserved by the
144 purification protocol, and/or the interaction is too transient and only occurs under certain
145 growth conditions. To better understand how CisA may be involved in mediating CIS^{Sc}
146 function, we set out to further characterize CisA *in vivo*.

147 ## CisA is a bitopic protein

148 Previous bioinformatic analyses[18,19] and Alphafold2 modeling of CisA (Fig. 3a) suggest that
149 CisA consists of a largely unstructured N-terminal region, a transmembrane segment, and a
150 conserved immunoglobulin-like (IgG) domain at the C-terminus. To characterize the
151 intracellular localization of CisA, we first generated a strain in which *cisA* was fused to the N-
152 terminus of *mcherry* and expressed *in trans* from a constitutive promoter in the
153 *S. coelicolor* Δ*cisA* mutant. Using fluorescence light microscopy, we consistently observed a
154 CisA-mCherry fluorescence signal along the hyphal periphery, indicative of a membrane-
155 associated protein (Fig. 3b). In contrast, no fluorescence was observed in WT hyphae carrying
156 an empty plasmid (Fig. 3c). In furtherance to this, we wanted to provide more support that
157 CisA localized to the membrane and so, we performed cellular fractionation experiments to
158 separate soluble proteins from membrane proteins using whole cell lysates from the *S.*
159 *coelicolor* WT or from the Δ*cisA* mutant that was complemented with a *cisA-3xFLAG* fusion
160 expressed *in trans* from a constitutive promoter. Our analysis confirmed that CisA-3xFLAG
161 co-sedimented with the cell membranes, while the cytoplasmic transcription factor WhiA could
162 only be detected in the soluble protein fraction (Fig. 3d).

163 Next, we investigated the topology of CisA in the membrane by using a dual *phoA-lacZα*
164 reporter system in *E. coli*. The reporter activity can be directly visualized on indicator plates
165 based on the complementary activities of the cytoplasmic reporter β-galactosidase LacZ
166 (magenta coloration) and the periplasmic reporter alkaline phosphatase PhoA (blue
167 coloration)[27]. We engineered *E. coli* strains that expressed a C-terminal fusion of CisA variants
168 to the PhoA-LacZα reporter, including full-length CisA and CisA variants that carried either a
169 deletion in the predicted transmembrane domain and/or the putative periplasmic domain (Fig.
170 3e). In addition, we included three controls, including cells 1) carrying the empty reporter
171 plasmid, resulting only in cytoplasmic β-galactosidase activity, and expressing a PhoA/LacZ
172 fusion to 2) the *Streptomyces* cytoplasmic cell division protein SepH and 3) the periplasmic
173 domain of the *Streptomyces* membrane protein RsbN[28,29]. The results of this assay confirmed
174 that CisA is a bitopic protein with an N-terminus (amino acids 1-285) located in the cytoplasm
175 and a C-terminus (amino acids 310-468) present in the periplasm of *E. coli* (Fig. 3f).

176 Collectively, our results demonstrate that CisA is a membrane protein comprised of a flexible,
177 cytoplasmic N-terminal domain and a C-terminal globular IgG-like domain that is exposed to
178 the outside of the cytoplasmic membrane.

179 CisA is essential for the cellular function of CIS^{Sc}

180 We previously established a fluorescence-based assay to demonstrate that the production of
181 functional CIS^{Sc} particles results in a significantly reduced viability of *Streptomyces* hyphae
182 that were exposed to exogenous stress, including treatment with the membrane-pore forming
183 antibiotic nisin, UV radiation or the protonophore carbonyl cyanide 3-chlorophenylhydrazone
184 (CCCP)[18]. The assay is based on the measurement of the ratio of two fluorescent markers,
185 namely cytoplasmic sfGFP produced by viable intact hyphae and the membrane dye FM5-95
186 to detect intact as well as partially lysed hyphae. Using this assay, we tested whether CisA was
187 essential for CIS^{Sc}-mediated cell death. We therefore determined the relative viability of the
188 WT *cisA*, the Δ*cisA* and the complemented *cisA* (Δ*cisA/cisA*$^{+}$) strains expressing cytosolic
189 sfGFP. We compared cells that were exposed to a sublethal concentration of nisin (1 µg/ml for
190 90 min) to cells that were not exposed to antibiotic stress. All three strains were found to
191 express CIS^{Sc} assemblies under these growth conditions (EV6).

192 In the absence of nisin stress, all three strains exhibited a similar sfGFP/FM5-95 ratio,
193 indicating no significant difference in viability (Fig. 4a/c). As previously observed[18], the
194 viability of the WT was dramatically reduced in response to nisin stress. In contrast, the
195 viability of Δ*cisA* hyphae was unaffected by nisin stress and comparable to the viability of
196 untreated cells. This phenotype could be completely reversed by complementing the Δ*cisA*
197 deletion *in trans* (Fig. 4b/d). Notably, the Δ*cisA* strain phenocopies CIS^{Sc} knockout and non-
198 contractile mutants that we analyzed previously[18]. Thus, we conclude that CisA is required for
199 CIS^{Sc}-mediated cell death upon stress.

200 To further test the dependence of CIS^{Sc} function on CisA, we conducted additional *in vivo*
201 assays. Previous studies showed that the absence of functional CIS^{Sc} impacted the timely
202 differentiation of *Streptomyces* hyphae into chains of spores, resulting in accelerated cellular
203 development and reduced secondary metabolite production[18,19]. Here we repeated these
204 analyses using the WT, the Δ*cisA* mutant and the complemented mutant (Δ*cisA/cisA*$^{+}$). All
205 strains consistently completed their life cycle and synthesized spores after 96 h of growth on

206 solid medium (Fig. 4e). Importantly, unlike the WT and the Δ*cisA/cisA*$^{+}$strain, Δ*cisA* mutant
207 colonies sporulated markedly earlier (72 h). These findings were further corroborated by
208 quantifying the number of spores produced by each strain under the same experimental
209 conditions (Fig. 4f). Finally, we also tested the production of the two characteristic pigmented
210 secondary metabolites of *S. coelicolor*, actinorhodin (blue)[30] and undecylprodigiosin (red)[31].
211 Compared to the WT and the Δ*cisA/cisA*$^{+}$ strain, the Δ*cisA* mutant showed significantly
212 reduced levels of secondary metabolite production (EV7). Our data therefore support the
213 conclusion that the cellular function of CIS^{Sc} in *S. coelicolor* is dependent on CisA and its
214 absence impacts the timely cellular and chemical differentiation of *S. coelicolor* hyphae.

215 # Conclusion

216 Here we identify CisA as an essential membrane-associated factor that mediates the cellular
217 function of CIS^{Sc} particles in *Streptomyces coelicolor*. In the absence of CisA, CIS^{Sc} are not
218 able to contract in the cellular context (Fig. 1). Similar to a CIS^{Sc} deletion or non-contractile
219 mutant[18], this decreases the induction of regulated cell death upon stress, which in turn affects
220 cellular development and secondary metabolite production (Fig. 5). The mechanistic aspects
221 of this distinct mode of action of a CIS are discussed further below.

222 A conserved feature of all previously studied CIS is the requirement of the contractile apparatus
223 to bind to a membrane before firing. This can be achieved in different ways, leading to the
224 classification of CIS into different modes of action. First, T6SS are anchored to the cytoplasmic
225 membrane of the host cell by a trans-envelope complex spanning from the cytoplasm to the
226 inner membrane, periplasm, and outer membrane[32–34]. Second, contractile phages and eCIS
227 bind to the surface of their target cell via tail fibers, which are typically connected to the
228 baseplate and transmit the signal for firing to the baseplate[13,16,35]. Third, tCIS are anchored to
229 thylakoid membrane stacks in cyanobacteria by an extension of their baseplate[36]. Our data
230 suggest that CisA may be required to mediate an interaction of CIS^{Sc} with the cytoplasmic
231 membrane prior to firing. This interaction may occur directly via the binding of the CIS^{Sc}
232 particle to the membrane protein CisA, or through the interaction with a yet unknown factor.
233 We performed an *in silico* prediction of protein-protein interactions between CisA and CIS^{Sc}
234 components using Alphafold2-Multimer. Interestingly, this analysis identified Cis11 as a
235 significant hit, suggesting the possibility of a direct interaction of CisA with Cis11 (EV8a).
236 Such a protein-protein interaction would be consistent with our cryoEM structure, showing a
237 peripheral surface-exposed position of Cis11 within the baseplate (EV8b). We were unable,
238 however, to confirm a direct interaction between CisA and Cis11 *in vivo* by co-
239 immunoprecipitation with and without nisin stress. We did also not detect CisA in our CIS^{Sc}
240 purifications that were used for structure determination (Fig. 2). Importantly, however, by
241 proteomics we did detect CisA peptides in a crude purification of CIS^{Sc} from nisin-stressed
242 cells (Table EV2). This would be consistent with a transient and/or short-lived interaction of
243 CIS^{Sc} particles with CisA triggered by an exogenous or cellular signal. In agreement with this
244 idea, we rarely observed extended CIS^{Sc} assemblies that were associated with the membrane
245 via their baseplate in WT cells (Fig. 1d).

246 We speculate that CisA may not only serve as a mediator for the interaction of CIS^{Sc} with the
247 cytoplasmic membrane but also as a sensor and checkpoint for inducing cell death only under
248 specific stress conditions or in response to cellular signals. The CisA C-terminal IgG-like
249 domain that is localized outside the cytoplasm and in proximity of the Gram-positive cell wall
250 may sense stress signals that could potentially trigger conformational changes in CisA which
251 in turn could mediate the recruitment of CIS^{Sc} assemblies to the cytoplasmic membrane,
252 followed by firing. The fatal outcome of firing for the producing cell may have driven the
253 evolution of a stepwise mechanism involving a checkpoint that prevents self-inflicted cell death
254 by accidental firing. Such a mechanism would keep the CIS^{Sc} in a free-floating, non-functional
255 and safe state in the cytoplasm.

256 # METHODS

257 ## Bacterial strains, plasmids, and oligonucleotides

258 Bacterial strains, plasmids, and oligonucleotides used in this study are listed in Supplementary
259 Tables 3-4. Plasmids were generated using either standard restriction-ligation or assembled
260 using the Gibson Assembly Master Mix (NEB) or *In Vivo* Assembly. All plasmids were
261 verified by DNA sequencing. *Escherichia coli* strains were cultured in LB, SOB, or DNA
262 medium. *E. coli* strains TOP10, DH5α and NEB5α were used to propagate plasmids and
263 cosmids, *E. coli* strain BW25113/pIJ790 for recombineering cosmids and *E. coli*
264 ET12567/pUZ8002 for interspecies conjugation. When required, media was supplemented
265 with antibiotics at the following concentrations: 100 µg/ml carbenicillin, 50 µg/ml apramycin,
266 50 µg/ml kanamycin, 50 µg/ml hygromycin.

267 *Streptomyces coelicolor* strains were cultivated in LB, TSB, TSB-YEME, or R2YE liquid
268 medium at 30 °C in baffled flasks or flasks with springs, at 250 rpm or grown on LB, SFM,
269 R2YE medium solidified with 1.5 % (w/v) Difco agar[37]. Antibiotics were added at the
270 following concentrations: 25 µg/ml apramycin, 50 µg/ml kanamycin, 25 µg/ml hygromycin,
271 12.5 µg/ml nalidixic acid.

272 ## Construction of the *S. coelicolor* Δ*cisA* mutant

273 The λ RED homologous recombination system was used to isolate gene replacement mutations
274 using PCR-directed mutagenesis (ReDirect) of the *S. coelicolor* cosmid StD8A containing the
275 *cis* gene cluster[38,39]. The *cisA* coding sequence (*SCO4242*) was replaced with the *aac3(IV)-*
276 *oriT* resistance cassette from pIJ773. The mutant cosmid (pSS684) was introduced into *E. coli*
277 ET12567/pUZ8002, followed by conjugation into *S. coelicolor* M145. Exconjugants that had
278 successfully undergone double-homologous recombination were identified by screening for
279 apramycin resistance and kanamycin sensitivity. The deletion of *cisA* was subsequently verified by
280 PCR.

281 ## Sheath preparation of CIS^{Sc}

282 *S. coelicolor* strains were grown in 30 ml TSB, TSB-YEME or R2YE liquid medium for 48 h.
283 Cells were pelleted by centrifugation (7,000 x g, 10 min, 4 °C), resuspended in 5 ml lysis buffer

284 (150 mM NaCl, 50 mM Tris-HCl, 0.5× CellLytic B (Sigma-Aldrich), 1 % Triton X 100, 200
285 µg/ml lysozyme, 50 µg/ml DNAse I, pH 7.4), and incubated for 1 h at 37 °C. Cell debris was
286 removed by centrifugation (15,000 × g, 15 min, 4 °C) and cleared lysates were subjected to
287 ultra-centrifugation (150,000 × g, 1 h, 4 °C). Pellets were resuspended in 150 µl resuspension
288 buffer (150 mM NaCl, 50 mM Tris-HCl, supplemented with protease inhibitor cocktail
289 [Roche], pH 7.4). CIS^{Sc} sheath preparations were analyzed by negative stain EM imaging[40] and
290 mass spectrometry at the Functional Genomics Center Zürich.

291 To purify non-contractile CIS^{Sc} particles from *S. coelicolor (*SS393*)*, cleared cell lysates were
292 subjected to ultracentrifugation using a sucrose cushion (20 mM Tris pH 8.0, 150 mM NaCl,
293 50 mM EDTA, 1 % Triton X 100, 50 % [w/v] sucrose)[18]. The sucrose cushion alongside 1 mm
294 of liquid above and residual bacterial contaminants were removed by centrifugation at 15,000
295 x g. Samples were then subjected to a second round of ultracentrifugation without a sucrose
296 cushion (150,000 × g, 1 h, 4 °C) and resulting cell pellets were resuspended in buffer (50 mM
297 Tris, 150 mM NaCl). These crude samples were then purified further by gradient
298 ultracentrifugation (10 %-50 % continuous gradient made with BIOCOMP gradient master IP
299 model 107 gradient forming instrument) at 100,000 x g for 1 h using a SW55 Ti rotor. The
300 gradient was analyzed in 11 fractions of 500 µl and checked by negative stain EM. The
301 fractions, which contained CIS^{Sc} particles, were pooled and used for further experiments.

302 Negative stain electron microscopy

303 4 µl of purified CIS^{Sc} sheath particles were adsorbed to glow-discharged, carbon-coated copper
304 grids (Electron Microscopy Sciences) for 60 s, washed twice with milli-Q water and stained
305 with 2 % phosphotungstic acid for 45 s. The grids were imaged at room temperature using a
306 Thermo Fisher Scientific Morgagni transmission electron microscope (TEM) operated at
307 80 kV.

308 Mass spectrometry analysis

309 To confirm the presence of predicted CIS^{Sc} components, isolated sheath particles were
310 subjected to liquid chromatography–mass spectrometry analysis (LC–MS/MS). These
311 experiments were conducted at the Functional Genomics Center Zürich. First, the samples were
312 digested with 5 µl of trypsin (100 ng/µl in 10 mM HCl) and microwaved for 30 min at 60 °C.

313 The samples were then dried, dissolved in 20 µl ddH_20 with 0.1 % formic acid, diluted in 1:10
314 and transferred to autosampler vials for liquid chromatography with tandem mass spectrometry
315 analysis. A total of 1 µl was injected on a nanoAcquity UPLC coupled to a Q-Exactive mass
316 spectrometer (ThermoFisher). Database searches were performed by using the Mascot
317 swissprot and tremble_streptomycetes search programs. For search results, stringent settings
318 have been applied in Scaffold (1 % protein false discovery rate, a minimum of two peptides
319 per protein, 0.1 % peptide false discovery rate). The results were visualized by Scaffold
320 software ([Proteome Software Inc.], Version 4.11.1).

321 Protein gel electrophoresis and western blotting

322 For general protein analysis, protein samples were boiled at 95 °C for 5 min and separated by
323 a 4–20% Mini-PROTEAN® TGX Stain-Free™ SDS PAGE (BioRad) or 12 % Tris-Glycine
324 SDS PAGA (Invitrogen) and visualized using InstantBlue Coomassie Protein Stain or
325 ReadyBlue Protein Gel Stain (Sigma Aldrich).

326 For western blotting, cells were grown in biological triplicate for 48 h in TSB, 2 ml aliquots of
327 each culture were pelleted and washed once with 1x PBS. Cell pellets were resuspended in 0.4
328 ml of sonication buffer (20 mM Tris pH 8.0, 5 mM EDTA, 1x EDTA-free protease inhibitors
329 [Sigma Aldrich]) and subjected to sonication at 4.5-micron amplitude for 7 cycles of 15 s on /
330 15 s off. Samples were centrifuged at 17,000 x *g* for 15 min at 4 °C. Protein concentration in
331 cleared cell lysate supernatants was determined by Bradford Assay (Biorad). Equivalent total
332 protein concentrations (1 mg/ml) were assayed using the semi-dry western blot transfer. The
333 gel was transferred to a PVDF membrane (Biorad) and probed with the appropriate antibody
334 diluted in TBS-T or using the iBIND buffer system (Thermo Fisher): Rabbit anti-FLAG
335 ([Sigma Aldrich] F7425, 1:2500), Rabbit anti-WhiA ([41], 1:2500), and Goat Anti-Rabbit-HRP
336 (Abcam Ab6721, 1:5000). To visualize HRP-conjugated antibodies, membranes were
337 incubated with SuperSignal West Femto ECL solution (Thermo Fisher).
338

339

340

341 ## Cellular fractionation

342 To fractionate membrane and soluble proteins from *S. coelicolor* (WT, SS576), cells were
343 grown for 48 h in 50 ml TSB/YEME and harvested by centrifugation. Cell pellets were
344 resuspended in 1/10 volume of lysis buffer (0.2 M Tris-HCl, pH 8, 10 mg/mL lysozyme, and
345 1× EDTA-free protease inhibitors; [Roche]), incubated for 30 min at 37 °C, and then briefly
346 cooled on ice before lysed by sonication (11 x 15 sec on/off at 50 % power at 8 microns on
347 ice). Cell debris was removed by centrifugation at 16,000 × g for 20 min and supernatant was
348 subsequently subjected to two additional rounds of centrifugation. The cleared cell lysate was
349 subjected to ultracentrifugation for 1 h at 150,000 × g at 4 °C to separate the soluble proteins
350 from membrane proteins. Sedimented membrane proteins were resuspended and washed twice
351 in 1 volume of wash buffer (60 mM Tris-HCl, 200 mM NaCl, pH 8, 0.2 mM EDTA, and 0.2
352 M sucrose) at 150,000 × g at 4 °C for 1 h. The wash step was repeated one final time with the
353 wash buffer containing 8 M urea to remove traces of membrane-associated proteins[42]. The final
354 pellet was dissolved in 1/10 of the initial volume with wash buffer (no urea). Equi-volume
355 amounts of fractions were mixed with 2x SDS sample buffer and analyzed by immunoblotting.

356 ## Membrane protein topology analysis in *E. coli*

357 The coding sequence of CisA was inserted in the dual pho-lac reporter plasmid pKTop, which
358 consists of an *E. coli* alkaline phosphatase fragment $PhoA_{22-472}$ fused in frame after the α-
359 fragment of β-galactosidase $LacZ_{4-60}$ (Table EV3)[27]. For membrane protein topology, *E. coli*
360 TG1 was transformed with the pKTop and derivatives. Membrane protein topology was
361 assayed by plating the resulting reporter strains on dual-indicator plates containing LB agar
362 supplemented with 80 µg/ml 5-bromo-4-chloro-3-indolyl phosphate disodium salt (X-Phos)
363 ([Sigma Aldrich], RES1364C-A101X) and 100 µg/mL 6-chloro-3-indolyl-β-d-galactoside
364 (Red-Gal) ([Sigma Aldrich], B6149) as indicators, 1 mM IPTG, and 50 µg/ml kanamycin. A
365 periplasmic or extracellular location of the reporter fusion results in higher alkaline
366 phosphatase activity (blue color), whereas a cytosolic location of the reporter leads to higher
367 β-galactosidase activity (magenta color). Plates were incubated for two days at 37 °C and
368 scanned.
369

370

371 ## Vitrified sample preparations

372 For single-particle cryoEM (SPA), the *S. coelicolor* non-contractile CIS particles were purified
373 as described above and vitrified using a Vitrobot Mark IV (Thermo Fisher Scientific). 4 µl of
374 samples were applied twice on glow-discharged 200 mesh Quantifoil copper grids (R 2/2)
375 which were manually coated with a layer of 1 nm carbon. Grids were blotted for 5.5 s and
376 plunge-frozen in liquid ethane-propane mix (37 %/63 %). Frozen grids were stored in liquid
377 nitrogen until loading into the microscope.

378 For cryo-electron tomography (cryoET), *Streptomyces* cells were mixed with 10 nm Protein A
379 conjugated colloidal gold particles (1:10 v/v, [Cytodiagnostics]) and 4 µl of the mixture was
380 applied to a glow-discharged holey-carbon copper EM grid (R2/1 or R2/2, [Quantifoil]). The
381 grid was automatically blotted from the backside for 4-6 s in a Mark IV Vitrobot by using a
382 Teflon sheet on the front pad, and plunge-frozen in a liquid ethane-propane mixture (37 %/63
383 %) cooled by a liquid nitrogen bath.

384 ## SPA data collection and image processing

385 44,925 movies were collected on Titan Krios microscope (Thermo Fisher Scientific), operated
386 at 300 keV equipped with K3 direct electron detector, operating in counting mode, and using
387 a slit width of 20 eV on a GIF-Quantum energy filter (Gatan). The automated data collection
388 was conducted with EPU software (Thermo Fisher Scientific) with a final pixel size of
389 1.065Å/pix over 40 frames with a total dose of 50 $e^-/Å^2$. The targeted defocus was set between
390 -1.6 and -2.8 µm with 0.2 µm increment.

391 Movie-alignments with dose-weighting were performed in MotionCor2 software[43] with a gain
392 reference estimated a posteriori[44] followed by standard in-house pipeline of manual inspection
393 and selection of 38,845 micrographs[45] for further processing in cryoSPARC package v4.0.3[46].
394 Due to the low concentration of particles and the presence of other contaminants in the sample,
395 automatic particle picking appeared challenging, and we developed CIS-specific approach for
396 efficient picking of the cap and baseplates. In this approach, CIS^{Sc} particles were manually
397 selected as filaments (start-to-end) on 920 micrographs and used for training a crYOLO[47]
398 picking model (EV2). The large size of the training set appeared essential for successful
399 picking; we could not get rid of large number of false-positive picks, but there were not so
400 many false-negative picks. Then, CIS^{Sc} particles were picked in crYOLO as filaments,

401 followed by the extraction of the ends of the "filaments" using star_modif.py script[45]. Particle
402 coordinates were imported in cryoSPARC, where 211,041 particles were extracted at a large
403 box size of 756 pixels binned to 64 pixels for initial 2D-classification, which allowed us to
404 separate initial particle sets corresponding to the CIS^{Sc} cap (36,569 particles) and CIS^{Sc}
405 baseplate (43,087 particles) (EV2).

406 Two subsets of this dataset were processed in cryoSPARC separately. For the cap subset, a
407 standard cryoSPARC single-particle processing approach was applied, including gradual
408 iterative 2D-classification rounds, followed by selection of good classes and particle re-
409 extraction at finer sampling. The main challenge was the proper centering of the particles
410 selected on the end of elongated filament-like objects with repeating patterns (sheath-tube
411 module of CIS), hampering the alignments. Ab-initio model generation with applied C6
412 symmetry was hampered by poor centering of 2D-classes due to elongated nature of the
413 particles (EV2). Homo-refinement with this reference was performed followed by particle re-
414 extraction and one more round of ab-initio model generation with applied C6 symmetry (EV2).
415 The new 3D-reconstruction appeared reliable and was used for further iterative 3D-refinements
416 (Homo-refinement and NU-refinements) accompanied by 2D-classification and CTF-
417 refinement rounds to exclude particles with wrong Euler angle assignments. The final 3.4 Å
418 resolution map with imposed C6 symmetry resulted from 19,218 particles.

419 The baseplate subset was processed using the same approach, resulting in a 3D-reconstruction
420 with imposed C6 symmetry with a resolution of 3.5Å from 22,980 particles (EV2). The tip of
421 the baseplate has a C3 symmetry, therefore to solve that part of the map correctly, we exported
422 that particle stack to Relion4[48] and took advantage of 2D-classification in Relion to select
423 18,124 particles, corresponding to the best 2D classes averages. 3D-refinement with relaxed
424 symmetry resulted in a 3.8 Å 3D-resolution reconstruction with imposed C3 symmetry.

425 Cryo-electron tomography

426 Intact *Streptomyces* cells were imaged by cryoET as described previously[49]. Images were
427 recorded using a Titan Krios 300 kV microscope (Thermo Fisher Scientific) equipped with a
428 Quantum LS imaging filter operated at a 20 eV slit width and with K3 Summit direct electron
429 detectors (Gatan). Tilt series were collected using a bidirectional tilt-scheme from -60 to +60°
430 in 2° increments. Total dose was 130-150 $e^-/Å^2$ and defocus was kept at -8 µm. Tilt series were
431 acquired using SerialEM[50], drift-corrected using alignframes, and reconstructed using IMOD

432 program suite[51]. To enhance contrast, tomograms were deconvolved with a Wiener-like filter
433 'tom_deconv'[52].

434 Structural modeling

435 The map qualities of different modules of CIS^{Sc} (cap and baseplate) allowed for *de novo*
436 structural modelling (EV2-3). The atomic models of SCO4243-4248, SCO4252-4253 and
437 SCO4260 were built *de novo* using COOT[53]. The resulting models were iteratively refined
438 using RosettaCM[54] and real-space refinement implemented in PHENIX[55]. In cases where
439 protein domains could only be partially modeled, side chains were not assigned. Final model
440 validation was done using MolProbity[55] and correlation between models and the corresponding
441 maps were estimated using mtriage[55].

442 Fluorescence microscopy

443 Fluorescence-based cell viability assays were performed as described previously[18]. Briefly, to
444 produce cytoplasmic sfGFP in *Streptomyces*, the coding sequence for sfGFP was introduced
445 downstream of the constitutive promoter *ermE** on an integrating plasmid. The plasmid was
446 introduced by conjugation to *S. coelicolor* strains (SS430, SS575, SS576. An equal level of
447 cytoplasmic sfGFP in the different strains was confirmed by Western blotting (EV9).
448 *Streptomyces* strains were grown in 30 ml of TSB liquid culture at 30 ˚C with shaking at 250
449 rpm for 48 h. Where appropriate, nisin was added to a final concentration of 1 µg/ml 90 min
450 prior to imaging. One ml aliquots of each culture were centrifuged for 5 min at 15,000 x *g*,
451 washed twice with 1xPBS, resuspended in 1 ml of 1xPBS containing 5 µg/ml of the red-
452 fluorescent membrane dye FM5-95 (Invitrogen) and then incubated in the dark at room
453 temperature for 10 min followed by two wash steps with 1x PBS. Washed cell pellets were
454 resuspended in a total volume of 50 µl PBS and 10 µl of each sample was spotted onto 1 %
455 agar pads and subsequently imaged using the Thunder imager 3D cell culture microscope
456 (Leica). First, tile scan images were acquired using the Las X Navigator plug-in software (Leica
457 Application Suite X, Version 3.7.4.23463), and 100 regions of interest were picked manually.
458 Then Z-stack images were acquired using a HC PL APO 100x objective with the following
459 excitation wavelengths: GFP (475 nm) and TRX (555 nm). Images were processed using LasX
460 software to apply thunder processing and maximum projection and FIJI to create segmentation
461 and quantify the live (sfGFP)/total cells (FM5-95) area ratio[56]. Statistical analyses were

462 performed on data from biological triplicates (n=100 images for each experiment) using a one-
463 way ANOVA and Tukey's post-test in GraphPad Prism 9 (Version 9.3.1).

464 For imaging the subcellular localization of the CIS adaptor protein in *Streptomyces*, cells (strain
465 JS69 or *S. coelicolor* M145) were grown for 48 h in TSB/YEME liquid medium. Two µl of
466 each strain were spotted on 1 % agarose pads and subsequently imaged. Images were acquired
467 using a Zeiss Axio Observer Z.1 inverted epifluorescence microscope fitted with a sCMOS
468 camera (Hamamatsu Orca FLASH 4), a Zeiss Colibri 7 LED light source, and a Hamamatsu
469 Orca Flash 4.0v3 sCMOS camera. mCherry fluorescence was detected using an
470 excitation/emission bandwidth of 577–603 nm/614–659 nm. Images were collected using Zen
471 Blue (Zeiss) and analyzed using Fiji[56].

472 Cover glass impression of *Streptomyces* spore chains

473 Spore titers of relevant strains were determined by dilution plating[18]. 10^7 colony forming units
474 (CFU) of *S. coelicolor* strains (WT, SS539, SS557) were spread onto R2YE agar plates and
475 grown at 30 °C. Sterile glass coverslips were gently applied to the top surface of each bacterial
476 lawn after 48 h, 72 h and 96 h post inoculation. Coverslips were then mounted onto glass
477 microscope slides and imaged using a 40x objective on a Leica Thunder Imager 3D Cell
478 Culture. Images were processed using FIJI[56].

479 Actinorhodin production assay

480 *S. coelicolor* strains (WT, SS539, SS557) were inoculated into 30 ml R2YE liquid media at a
481 final concentration of 1.5 x 10^6 CFU/ml. Cultures were grown in baffled flasks at 30 °C
482 overnight. Cultures were standardized to an OD_{450} of 0.5 and inoculated in 30 ml of fresh R2YE
483 liquid medium. For visual comparison of pigment production, images of the growing culture
484 were taken between t = 0 and t = 72 h (as indicated in EV7). For quantification of total
485 actinorhodin production, 480 µl of samples were collected at the same time points where
486 images were taken. 120 µl of 5M KOH was added, samples were vortexed and centrifuged at
487 5,000 x *g* for 5 min. The weight of each tube was recorded. A Synergy 2 plate reader (Biotek)
488 was used then to measure the absorbance of the supernatant at 640 nm. The absorbance was
489 normalized by the weight of the wet pellet.

490 Structure prediction

491 CisA structure was predicted using AlphaFold2[57] and further processed using UCSF Chimera[58]
492 or ChimeraX-1.7.1[59].

493 A pairwise *in silico* screen for possible interactions between CisA and components encoded by
494 the *S. coelicolor cis* gene cluster (*SCO4242-SCO4260*) was conducted using the AlphaFold2
495 Multimer-based LazyAF pipeline[57,60,61]. The confidence metric (ipTM) for the top model from
496 each pairwise interaction was tabulated and visualised using Prism (Version 10.2.2) with ipTM
497 scores >0.7, indicating a possible protein-protein interaction[62].

Data availability

Representative reconstructed tomograms (EMD-XXXXX, EMD-XXXXX, EMD-XXXXX, EMD-XXXXX, EMD-XXXXX, EMD-XXXXX, EMD-XXXXX…) and SPA cryoEM maps (EMD-XXXXX, EMD-XXXXX and EMD-XXXXX) have been deposited in the Electron Microscopy Data Bank. Atomic models (PDB: XXXX, PDB: XXXX, PDB: XXXX) have been deposited in the Protein Data Bank.

Acknowledgements

We thank ScopeM for instrument access at ETH Zürich. We thank the Functional Genomics Center Zürich for mass spectrometry support. Pilhofer Lab members are acknowledged for discussions. M.P. was supported by the Swiss National Science Foundation (31003A_179255/310030_212592), the European Research Council (679209), and the NOMIS foundation. Work in the lab of S.S. was supported by a Royal Society University Research Fellowship (URF\R1\180075) and BBSRC grant BB/T015349/1 to S.S. and by the BBSRC Institute Strategic Program grant BB/X01097X/1 to the John Innes Centre.

512 # Author contributions statement

513 B.C., S.S. and M.P. conceived the project. B.C. optimized the sample preparation for SPA;
514 B.C and P.A collected and processed the cryoEM data, reconstructed the cryoEM map; B.C,
515 P.E.H and J.X built and refined the structural models; B.C. and P.E.H conducted and processed
516 cryoET; B.C. conducted automated fluorescent light microscopy, determined sporulation
517 efficiency and actinorhodin production; J.W.S and S.S. generated plasmids and *Streptomyces*
518 strains; J.W.S. designed constructs and performed membrane topology assay. J.W.S. prepared
519 samples and performed cellular fractionation experiment. J.W.S. imaged strains expressing
520 fluorescently tagged CisA. B.C., J.W.S, S.S. and M.P. wrote the manuscript.

Competing interests statement

The authors declare no competing interests.

523 **Figures legends**

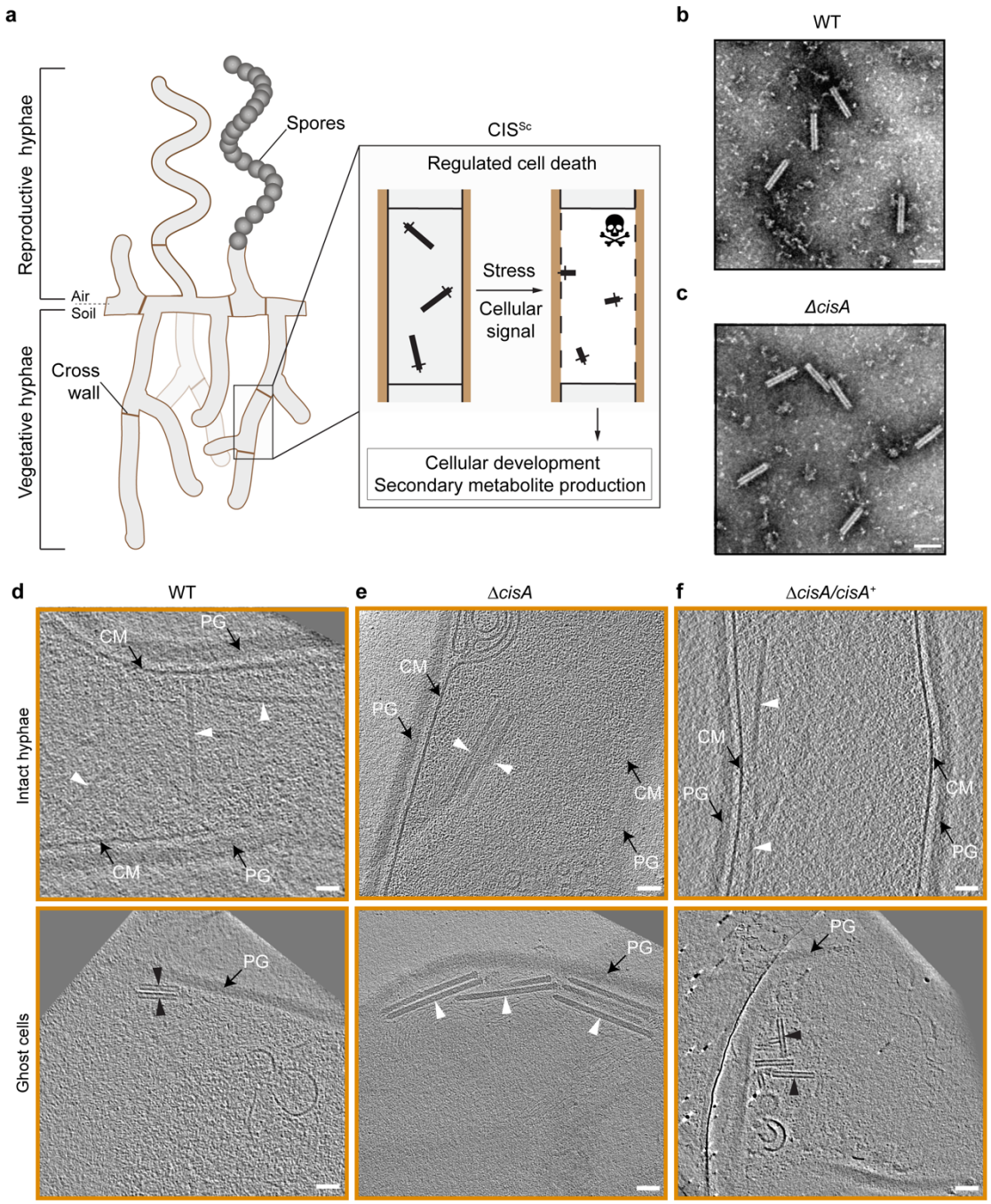

524

525 **Figure 1: Contraction of CIS^{Sc} *in situ* is dependent on CisA.**

526 **a.** Schematic of the mode of action of CIS^{Sc} in *Streptomyces coelicolor*[18,19]. CIS^{Sc} are assembled
527 as free-floating particles in the cytoplasm of vegetative hyphae. In response to cellular stress
528 and/or an unknown cellular signal, CIS^{Sc} particles contract, which results in regulated cell death
529 (mediated by released effectors) and impacts cellular development.

530 **b/c.** Negative-stain electron micrographs of purified CIS^{Sc} particles from *S. coelicolor* wildtype
531 (WT) (b) and the Δ*cisA* mutant (c), show that all CIS^{Sc} particles are contracted upon
532 purification. These experiments were performed three independent times. Bars, 100 nm.

533 **d-f.** Shown are representative images of cryo-electron tomogram slices (thickness 11 nm) of
534 vegetative hyphae (top: intact cells; bottom: ghost cells) of *S. coelicolor* WT (d), Δ*cisA* mutant
535 (e), and the complemented Δ*cisA/cisA*$^{+}$ mutant (f). CIS^{Sc} particles remain almost exclusively
536 in an extended state (white arrowheads) in the Δ*cisA* mutant, whereas in ghost cells derived
537 from the WT and the complemented mutant CIS^{Sc} particles (black arrowheads) are mostly
538 contracted. See also EV1. PG, peptidoglycan; CM, cytoplasmic membrane; Bars, 50 nm.

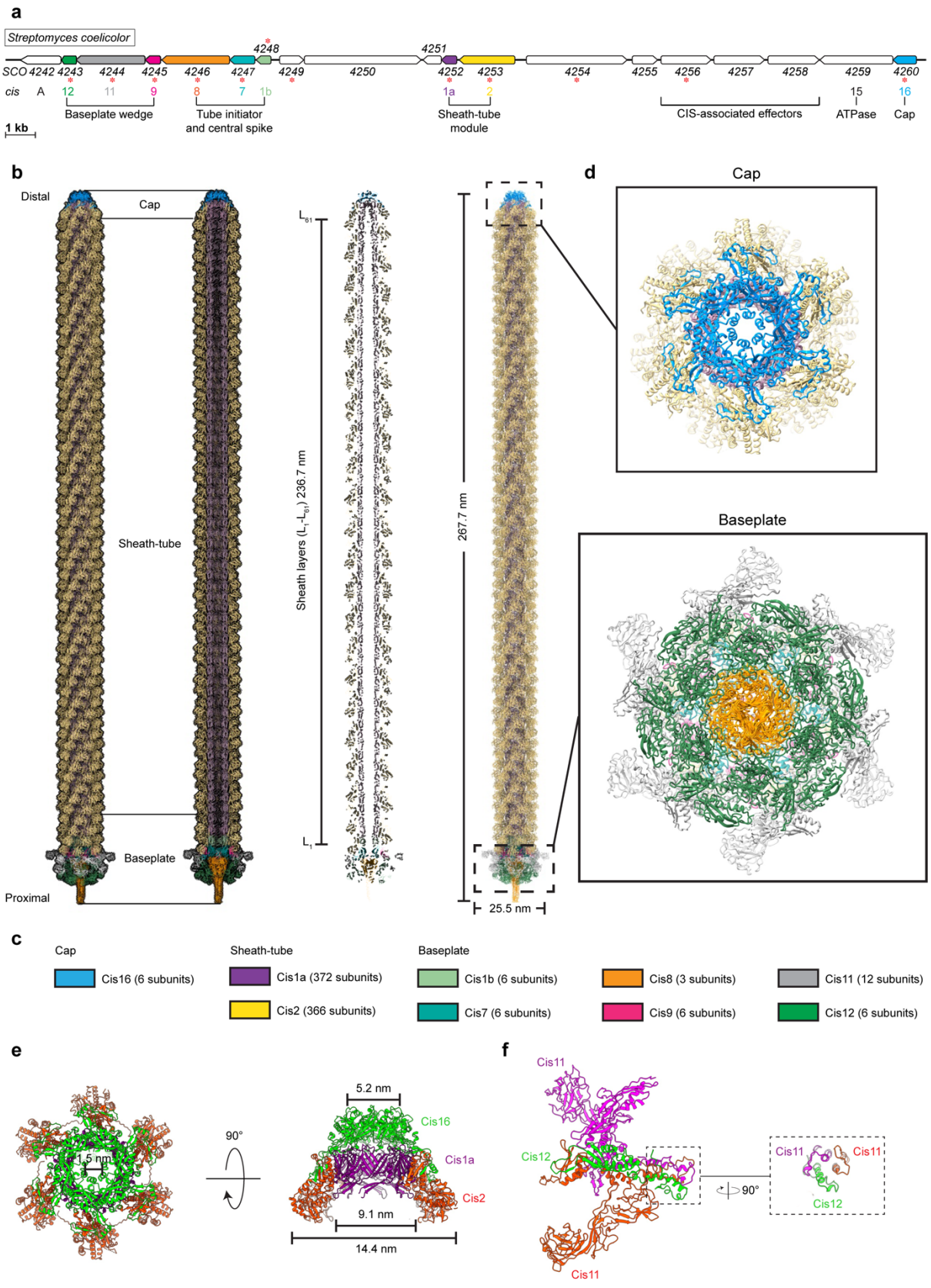
a
Streptomyces coelicolor
SCO 4242 4243 4244 4245 4246 4247 4248 4249 4250 4251 4252 4253 4254 4255 4256 4257 4258 4259 4260
cis A 12 11 9 8 7 1b 1a 2 15 16
Baseplate wedge
Tube initiator and central spike
Sheath-tube module
CIS-associated effectors
ATPase
Cap
1 kb
b
Distal
Cap
Sheath-tube
Baseplate
Proximal
Sheath layers (L1-L61) 236.7 nm
267.7 nm
25.5 nm
d
Cap
Baseplate
c
Cap
Cis16 (6 subunits)
Sheath-tube
Cis1a (372 subunits)
Cis2 (366 subunits)
Baseplate
Cis1b (6 subunits)
Cis7 (6 subunits)
Cis8 (3 subunits)
Cis9 (6 subunits)
Cis11 (12 subunits)
Cis12 (6 subunits)
e
1.5 nm
90°
5.2 nm
Cis16
Cis1a
Cis2
9.1 nm
14.4 nm
f
Cis11
Cis12
90°

541 **Figure 2: CryoEM structure of the extended CIS^{Sc} assembly reveals its composition.**

542 **a.** Schematic illustrating the CIS^{Sc} gene cluster (adapted from [18]). Asterisks indicate gene
543 products that were detected by mass spectrometry analyzing crude preparations of CIS^{Sc}
544 particles (red). See also Table EV1.

545 **b/c.** Single-particle cryoEM structure of an extended CIS^{Sc} particle obtained from purified
546 particles from a non-contractile CIS^{Sc} mutant. Shown is the composite atomic model in surface
547 (left) and ribbon (right) rendering (b). Subunits are color-coded according to (a) and their copy
548 numbers in the assembly are indicated in (c).

549 **d.** Perpendicular views of the ribbon representation of the CIS^{Sc} model of the cap and baseplate
550 modules.

551 **e.** Top view (left) and side view (right) of ribbon diagrams showing the cap module of CIS^{Sc},
552 revealing that the cap is composed of a Cis16 hexamer.

553 **f.** Ribbon diagrams showing a single baseplate wedge subunit, which is composed of two
554 copies of Cis11 and one copy of Cis12.

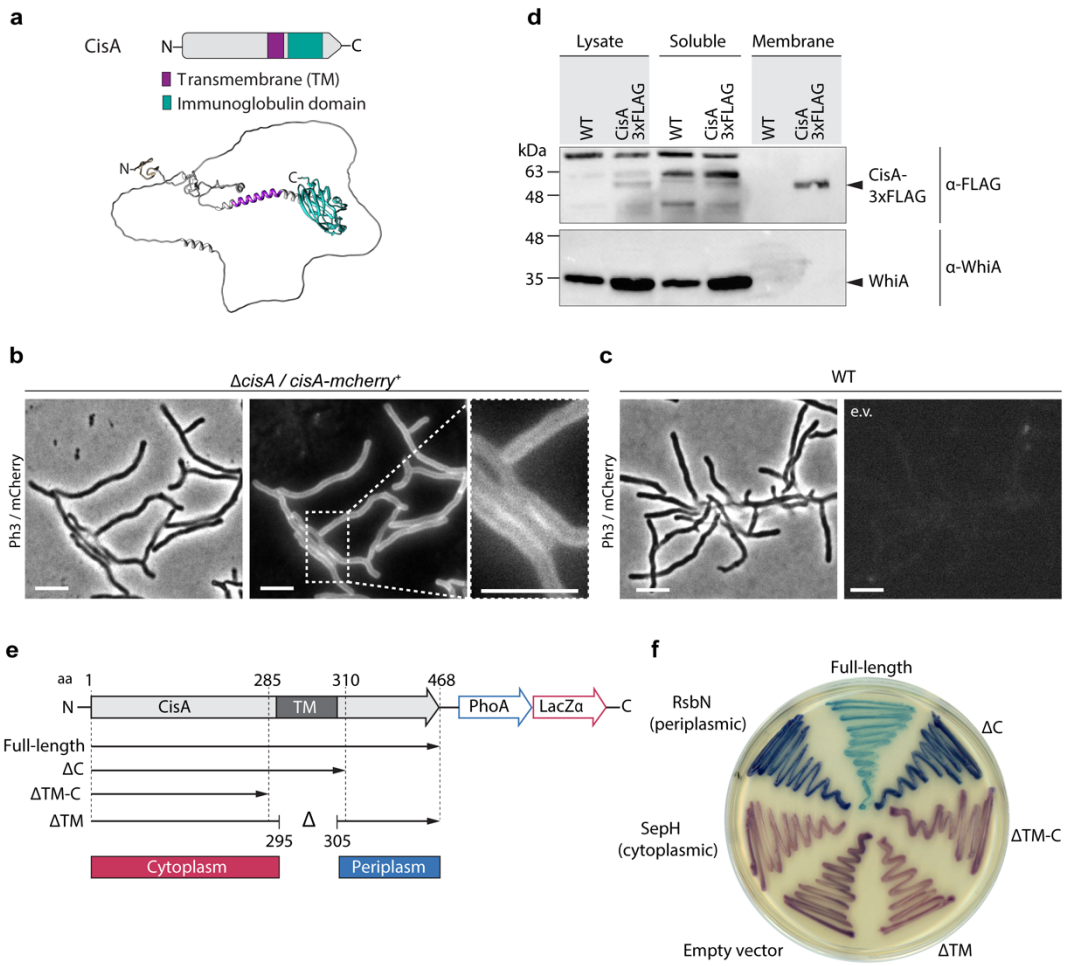

Figure 3: CisA is a single-pass membrane protein.

a. Schematic and Alphafold2 model of CisA. CisA is predicted to be comprised of a largely unstructured N-terminal domain (grey), a predicted transmembrane domain (TM, purple) and a C-terminal immunoglobulin-like domain (green)[18,19].

b/c. Representative micrographs (left panels: phase contrast, Ph3; right panel: mCherry) of strains of *S. coelicolor* vegetative hyphae either constitutively expressing CisA-mCherry (Δ*cisA/cisA-mcherry*) *in trans* (b) or WT cells carrying an empty vector (e.v.) to control for background fluorescence (c). Box shows a magnified region of hyphae with CisA-mCherry accumulation in the cellular periphery. Bars, 5 µm.

d. Western blot of the cellular fractionation of samples from the *S. coelicolor* WT or the Δ*cisA* mutant constitutively expressing a CisA-3xFLAG fusion *in trans*. Lysate and soluble and membrane fractions were probed for the presence of CisA-3xFLAG with an α-FLAG antibody

568 (top). Fractionation efficiency was assessed using an α-WhiA antibody to detect the soluble
569 transcription factor WhiA (bottom). CisA-3xFLAG was detected in the lysate and the
570 membrane fraction. The experiment was performed in biological duplicates and shown is a
571 representative image.

572 **e/f.** Experimental determination of the CisA membrane topology using the dual *phoA-lacZα*
573 reporter in *E. coli*. The schematic diagram (e) depicts the four CisA constructs used in the assay
574 and indicates the relevant amino acid (aa) deleted in the three CisA mutant derivates. The
575 analysis of colony coloration (f); pink coloration for cytosolic proteins and blue coloration for
576 periplasmic proteins indicates that the CisA N-terminus is localized in the cytoplasm and the
577 CisA C-terminus localized to the periplasm and this topology is dependent on the
578 transmembrane domain (TM). *E. coli* strains carrying an empty reporter plasmid or reporter
579 plasmids with the *Streptomyces* genes for SepH (cytoplasmic) and RsbN (periplasmic) were
580 used as controls. Note that expression of full-length CisA in *E. coli* is toxic, leading to reduced
581 growth and lighter blue coloration.

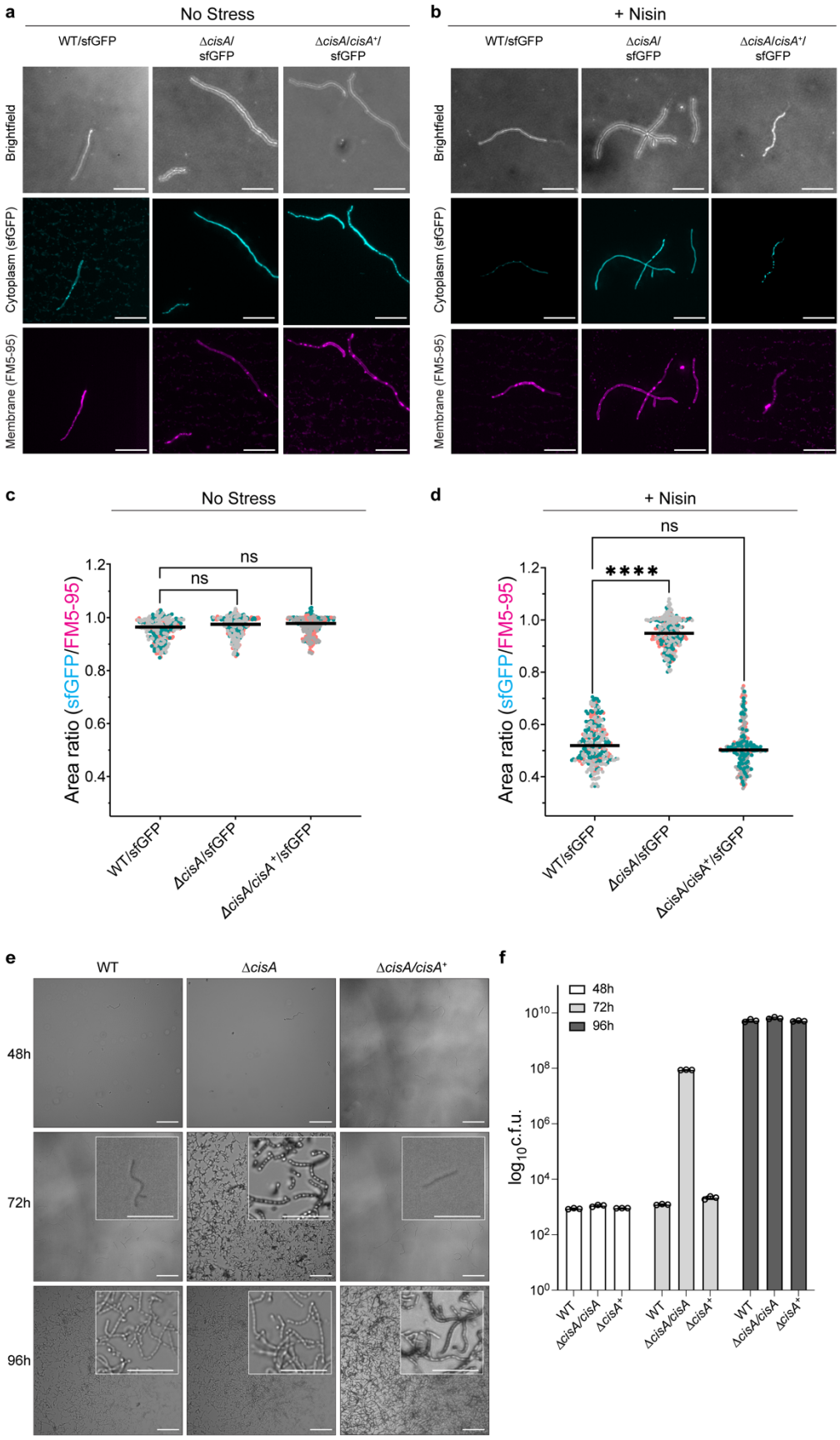
a
No Stress
WT/sfGFP
ΔcisA/ sfGFP
ΔcisA/cisA+/ sfGFP
Brightfield
Cytoplasm (sfGFP)
Membrane (FM5-95)
b
+ Nisin
c
d
Area ratio (sfGFP/FM5-95)
ns
****
WT/sfGFP
ΔcisA/sfGFP
ΔcisA/cisA+/sfGFP
e
WT
ΔcisA
ΔcisA/cisA+
48h
72h
96h
f
log10c.f.u.

582

583 **Figure 4: CisA is required for regulated cell death and cellular function of CIS^{Sc}.**

584 **a-d.** Light microscopy-based viability assay showing that CIS^{Sc} do not mediate cell death in
585 CisA-deficient hyphae in response to exogenous stress. Shown are representative micrographs
586 of the WT/sfGFP, the Δ*cisA*/sfGFP and the complemented Δ*cisA/cisA*$^{+}$/sfGFP mutant
587 expressing cytosolic sfGFP (indicator for live cells). Strains were grown for 48 h and then
588 either incubated without (a) or with (b) the membrane-disrupting antibiotic nisin (1 µg/ml nisin
589 for 90 min). Samples were subsequently stained with the fluorescent membrane dye FM5-95
590 to visualize the cytoplasmic membrane. Bars, 10 µm. Z-stacks were taken of the samples and
591 the relative ratio of fluorescence from sfGFP to FM5-95 was calculated in c/d. WT and
592 Δ*cisA/cisA*$^{+}$ complemented cells showed a significantly higher rate of cell death in response to
593 nisin treatment compared to Δ*cisA* cells. There is no significant difference in the viability of
594 the tested strains in the absence of nisin. Experiments were performed in three biological
595 replicates (green, grey and pink data points). Black lines indicate the mean ratio derived from
596 biological triplicate experiments (n=100 images per replicate). ns (not significant) and ****
597 ($p < 0.0001$) were determined using a one-way ANOVA and Tukey's post-test.

598 **e.** Visualization of spore production in WT, Δ*cisA* mutant and Δ*cisA/cisA*$^{+}$ mutant reveal
599 accelerated cellular development of the Δ*cisA* mutant. Shown are representative brightfield
600 images of surface impressions of plate-grown colonies of each of the strains taken at the
601 indicated time points. Only sporulating hyphae will attach to the hydrophobic cover glass
602 surface. Insets show magnified regions of the colony surface containing spores and spore
603 chains. Bars, 50 µm.

604 **f.** Quantification of sporulation shown in (e) via counts of colony-forming units (c.f.u.). The
605 graph shows a 6-fold higher c.f.u. count at 72 h in the Δ*cisA* mutant. Strains were grown on
606 R2YE agar and spores were harvested after 48 h, 72 h and 96 h of incubation. Data show mean
607 ± s.d. obtained from biological triplicate experiments.

608

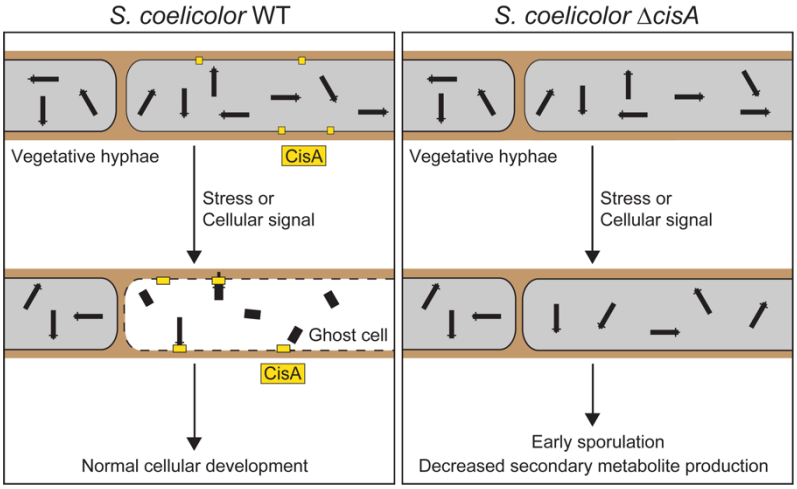

609 **Figure 5: Cytoplasmic CIS^{Sc} require the membrane protein CisA for contraction and**
610 **function.**

611 Proposed model illustrating a possible role of CisA. In response to exogenous stress or an
612 unknown cellular signal, membrane-bound CisA either directly or indirectly mediates the
613 association of free-floating CIS^{Sc} particles with the cytoplasmic membrane, leading to CIS^{Sc}
614 firing and regulated cell death, which impacts the *Streptomyces* developmental life cycle.

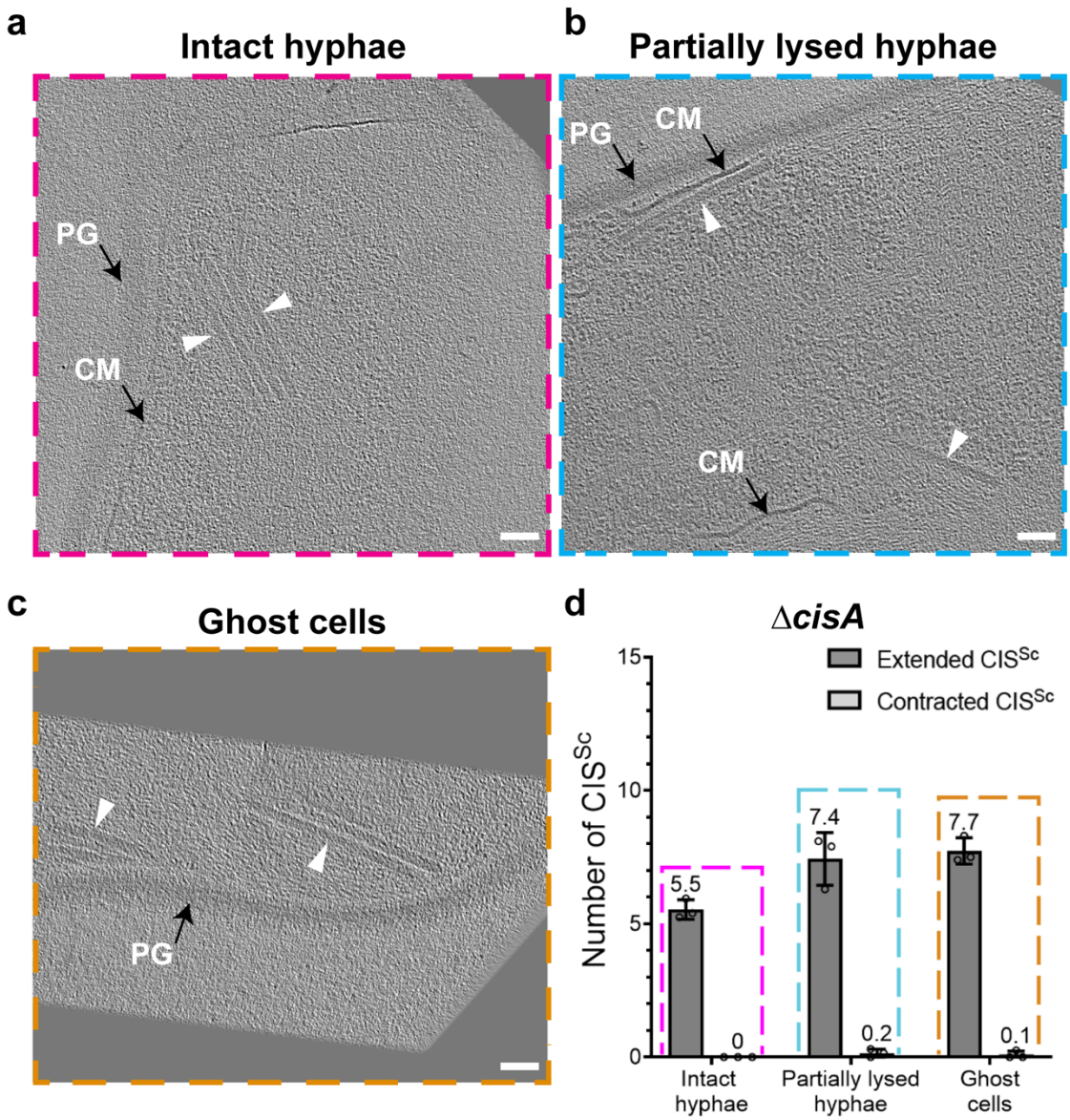

Extended Data Figure 1: Sheath contraction *in situ* is linked to the presence of CisA.

a-c. Shown are additional cryo-tomographic slices (thickness 11 nm) of *S. coelicolor* Δ*cisA* vegetative hyphae, which were observed as 'Intact hyphae' (a), 'Partially lysed hyphae' (b) and 'Ghost cells' (c). Note that all visible CIS^{Sc} particles (white arrowheads) are in the extended conformation. PG, peptidoglycan; CM, cytoplasmic membrane/membranes. Bars, 50 nm.

d. Shown is a quantification of CIS^{Sc} assemblies per tomogram and their conformations as observed in different classes of Δ*cisA* hyphae. Almost all CIS^{Sc} particles were seen in the extended conformation, indicating that sheath contraction *in situ* correlates with the presence of CisA. Data shows mean values and standard deviations obtained from biological triplicate experiments, with n=30 tomograms for each class of hyphae.

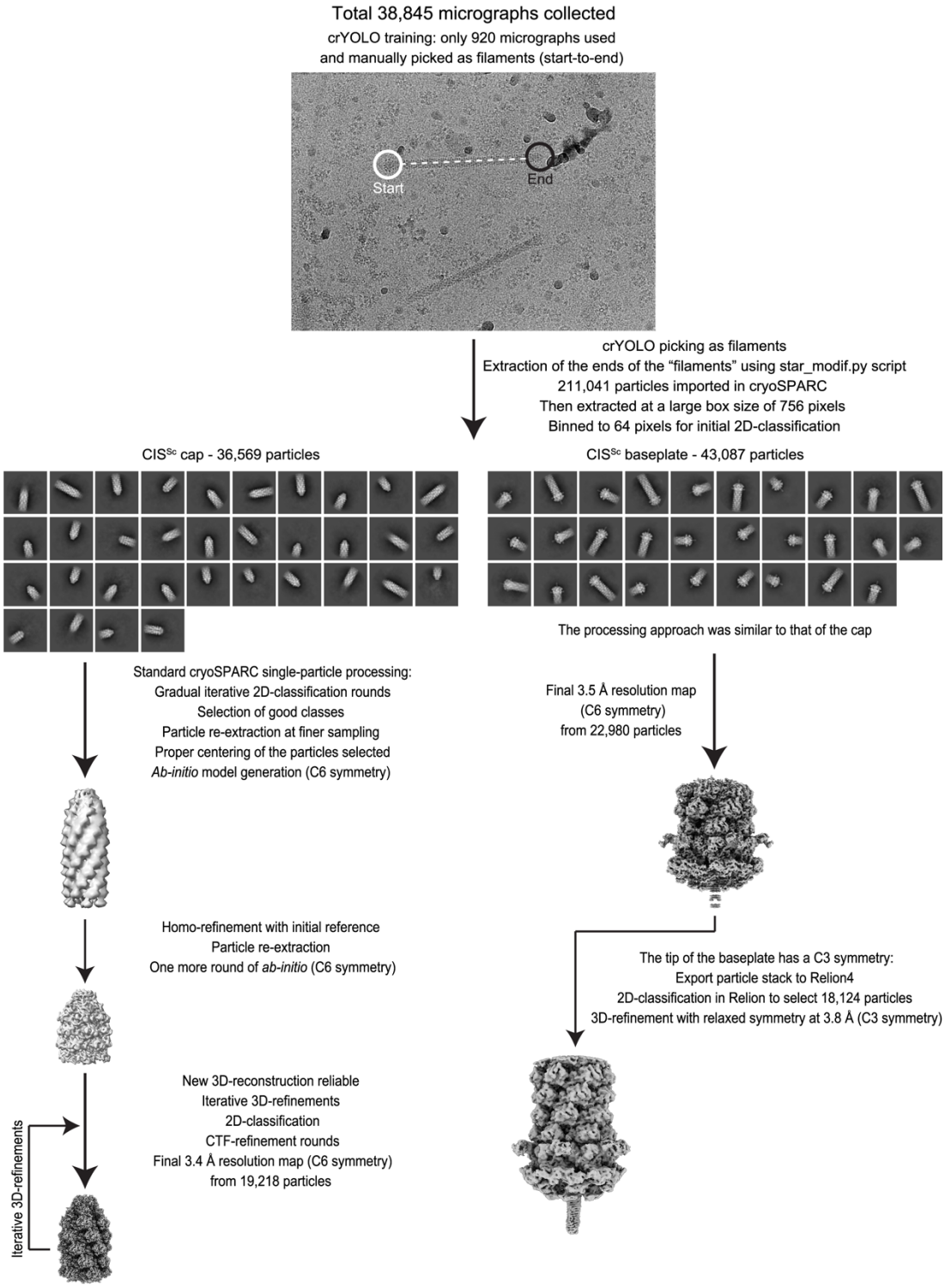

Extended Data Figure 2: Workflow for the cryoEM structural determination of the extended CIS^{Sc}.

Flowchart for cryoEM reconstruction of the extended CIS^{Sc} particle. See METHODS and Table EV1 for details.

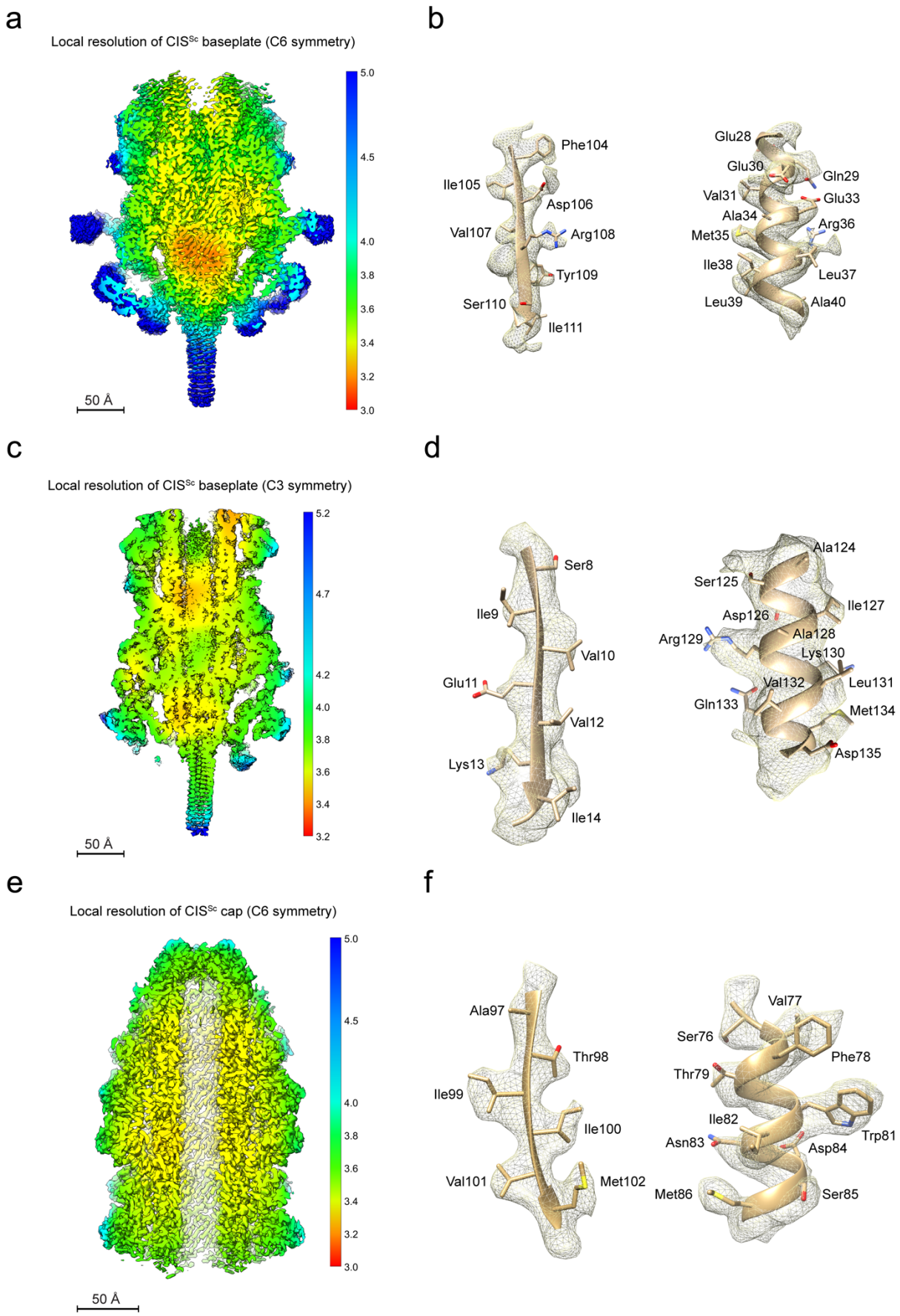
a
Local resolution of CIS^Sc baseplate (C6 symmetry)
5.0
4.5
4.0
3.8
3.6
3.4
3.2
3.0
50 Å
b
Phe104
Ile105
Asp106
Val107
Arg108
Tyr109
Ser110
Ile111
Glu28
Glu30
Gln29
Val31
Glu33
Ala34
Arg36
Met35
Ile38
Leu37
Leu39
Ala40
c
Local resolution of CIS^Sc baseplate (C3 symmetry)
5.2
4.7
4.2
4.0
3.8
3.6
3.4
3.2
50 Å
d
Ser8
Ile9
Val10
Glu11
Val12
Lys13
Ile14
Ala124
Ser125
Ile127
Asp126
Arg129
Ala128
Lys130
Leu131
Val132
Gln133
Met134
Asp135
e
Local resolution of CIS^Sc cap (C6 symmetry)
5.0
4.5
4.0
3.8
3.6
3.4
3.2
3.0
50 Å
f
Ala97
Thr98
Ile99
Ile100
Val101
Met102
Val77
Ser76
Phe78
Thr79
Ile82
Trp81
Asn83
Asp84
Met86
Ser85

631
632

633 **Extended Data Figure 3: Map qualities of different CIS^{Sc} modules.**

634 **a-f.** Local resolution maps of the CIS^{Sc} baseplate with C6 symmetry (a), CIS^{Sc} baseplate with
635 C3 symmetry (c), and the CIS^{Sc} cap with C6 symmetry (e). (d-f) shows regions of the cryoEM
636 density map (mesh) that were superimposed with the atomic models (ribbons and sticks),
637 demonstrating the agreement between the observed and modeled amino acid side chains for
638 one beta-sheet (left) and one alpha helix (right). Shown are examples of the baseplate with C6
639 symmetry (b), the baseplate with C3 symmetry (d), and the cap with C6 symmetry (f).

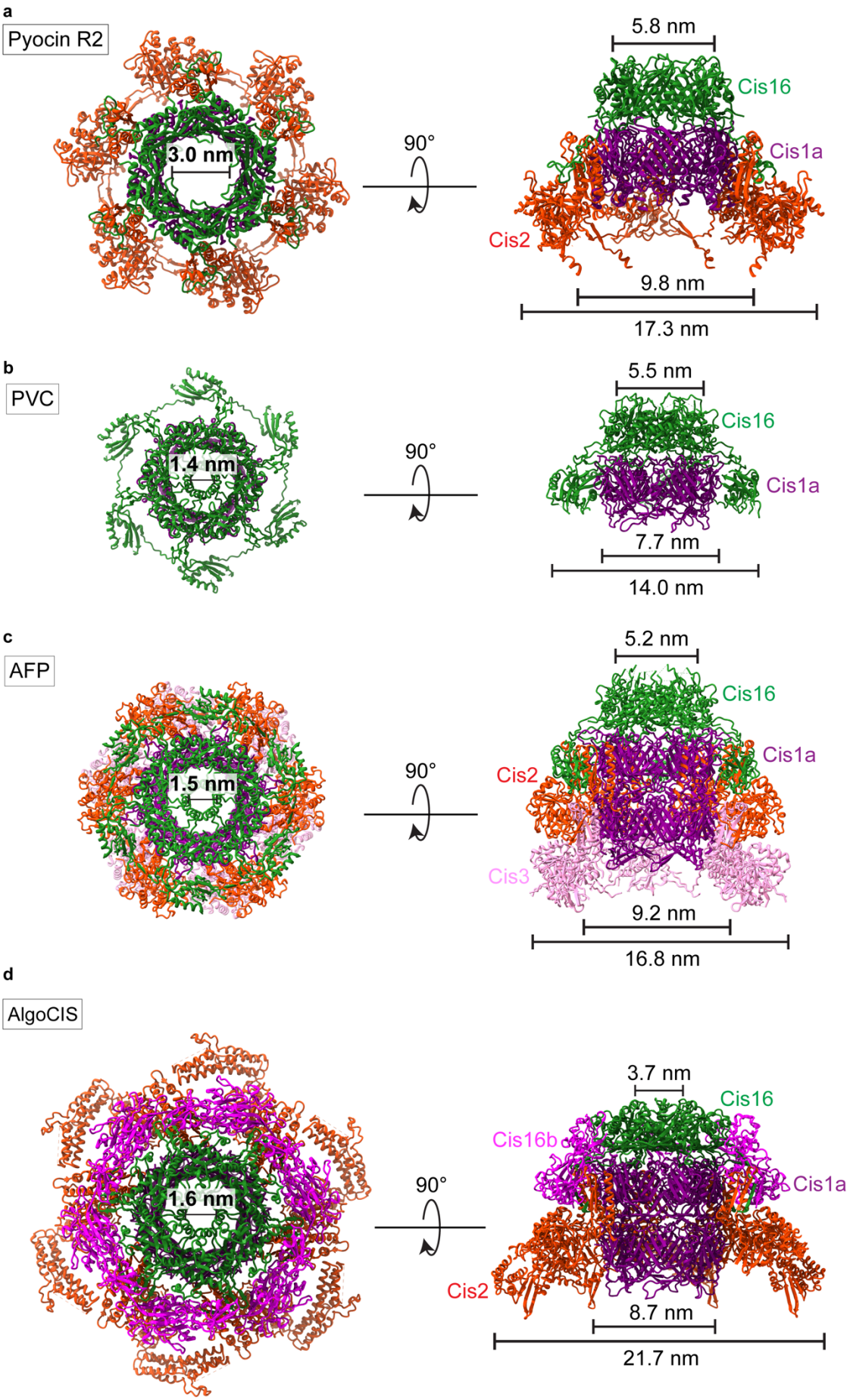
a
Pyocin R2
3.0 nm
90°
5.8 nm
Cis16
Cis1a
Cis2
9.8 nm
17.3 nm
b
PVC
1.4 nm
90°
5.5 nm
Cis16
Cis1a
7.7 nm
14.0 nm
c
AFP
1.5 nm
90°
5.2 nm
Cis16
Cis1a
Cis2
Cis3
9.2 nm
16.8 nm
d
AlgoCIS
1.6 nm
90°
3.7 nm
Cis16
Cis16b
Cis1a
Cis2
8.7 nm
21.7 nm

640

641 **Extended Data Figure 4: Structures of the cap modules of other CISs**.

642 **a-d.** Top views (left) and side views (right) of ribbon representations of the structures of CIS
643 cap modules of Pyocin R2 (a, PDB 6U5B), PVC (b, PDB 6J0N), AFP (**c**, PDB 6RAP) and
644 AlgoCIS (d, PDB 7ADZ).

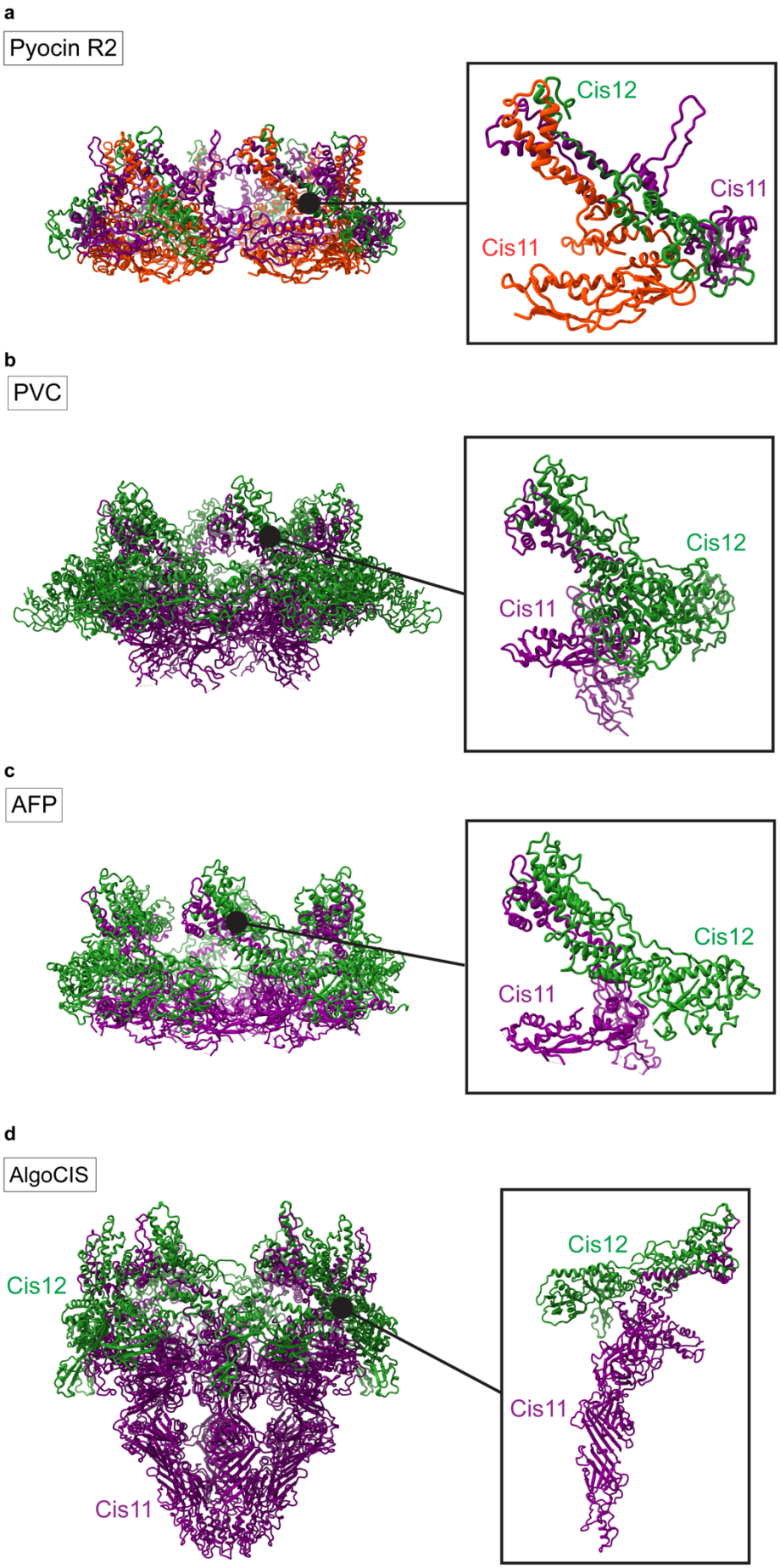
a
Pyocin R2
Cis12
Cis11
Cis11
b
PVC
Cis12
Cis11
c
AFP
Cis12
Cis11
d
AlgoCIS
Cis12
Cis11
Cis12
Cis11

645

646 **Extended Data Figure 5: Structures of the baseplate modules of other CISs**.

647 **a-d.** Ribbon representations of the full structures (left) and the individual wedge subunit (right)
648 of the CIS baseplate components (Cis11/12) of Pyocin R2 (a, PDB 6U5F), PVC (b, PDB 6J0F),
649 AFP (c, PDB 6RAO) and AlgoCIS (d, PDB 7AEB).

650

651

652

653

654

655

656

657

658

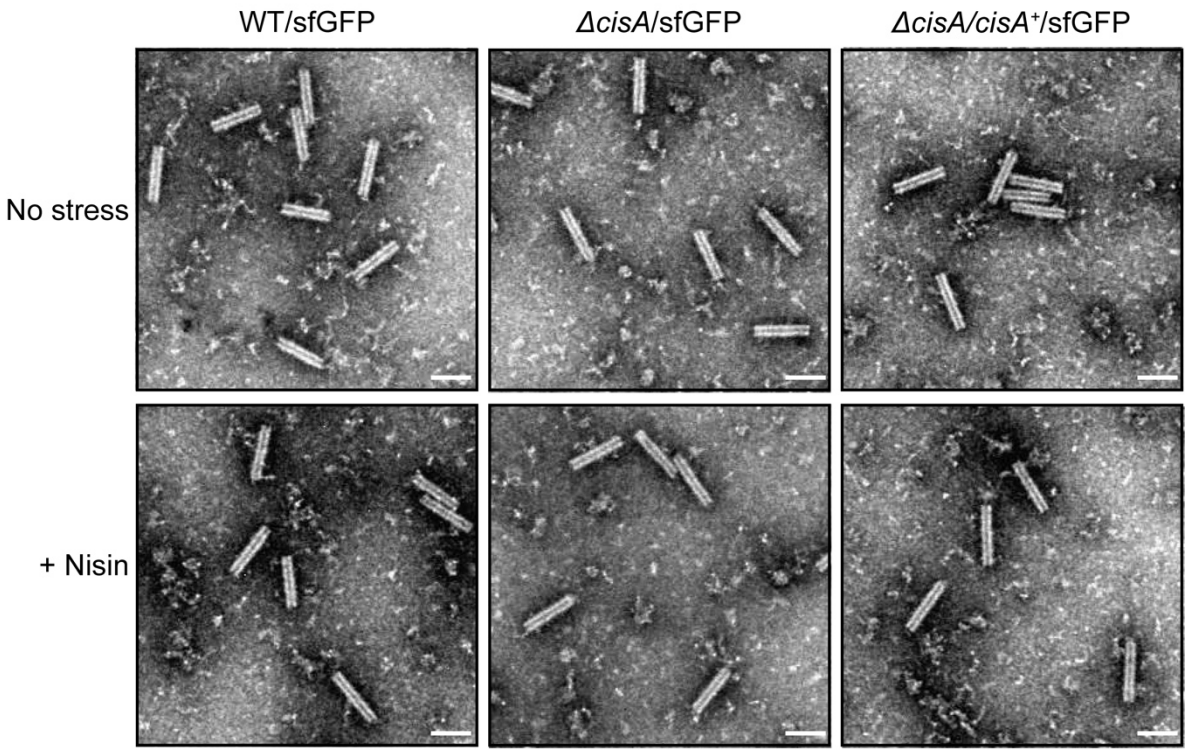

Extended Data Figure 6: Control experiment showing that CIS^{Sc} particles are comparable in the strains used in the viability assay.

Representative negative-stain electron micrographs of purified CIS^{Sc} particles from the WT/sfGFP, the Δ*cisA*/sfGFP mutant and the Δ*cisA*/Δ*cisA*$^{+}$/sfGFP complemented mutant exposed to no stress (upper row) or 1 µg/ml nisin (lower row). No differences were observed between the overall structure of CIS^{Sc} particles. These experiments were performed three independent times. Bars, 100 nm.

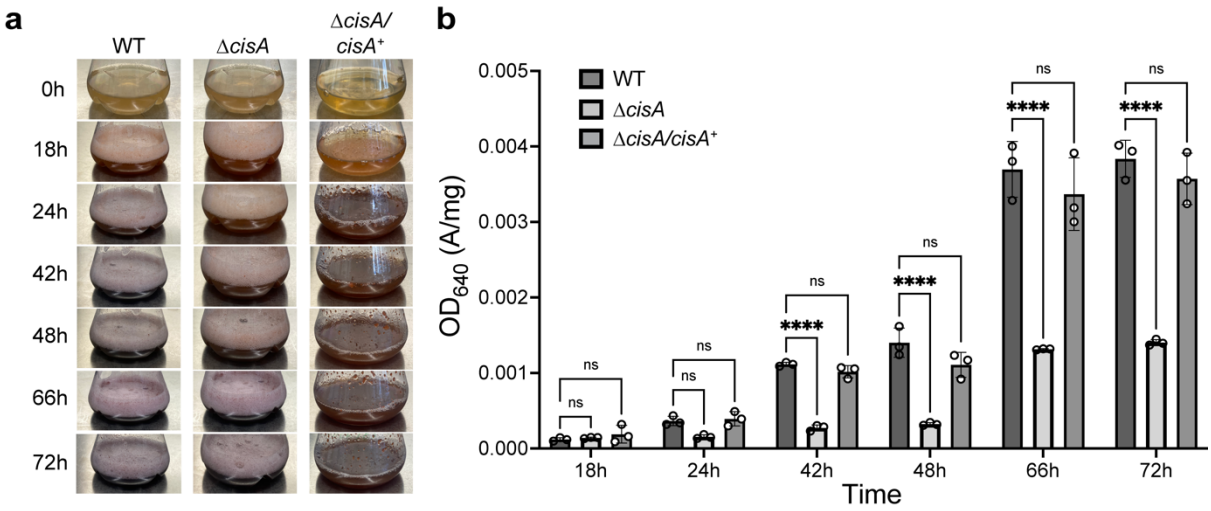

Extended Data Figure 7: CisA impacts secondary metabolite production.

a. Comparison of cultures of WT, Δ*cisA* mutant and Δ*c*isA/Δ*cisA*$^{+}$ mutant in R2YE liquid medium. The coloration of the culture is indicative of actinorhodin (purple) and undecylprodigiosin (red) production[31]. Images of each culture flask were taken at the indicated time points.

b. Quantification of total actinorhodin production by the strains shown in (a), revealing reduced production in the Δ*cisA* mutant. Samples were taken at the indicated time points. Actinorhodin was extracted and quantified by measuring the optical density OD_{640} of the culture supernatant[63] and normalized to the wet pellet weight. Analysis was performed in biological triplicate experiments. Shown are the mean values and standard error. ns (not significant) and **** ($p < 0.0001$) were calculated using one-way ANOVA and Tukey's post-test.

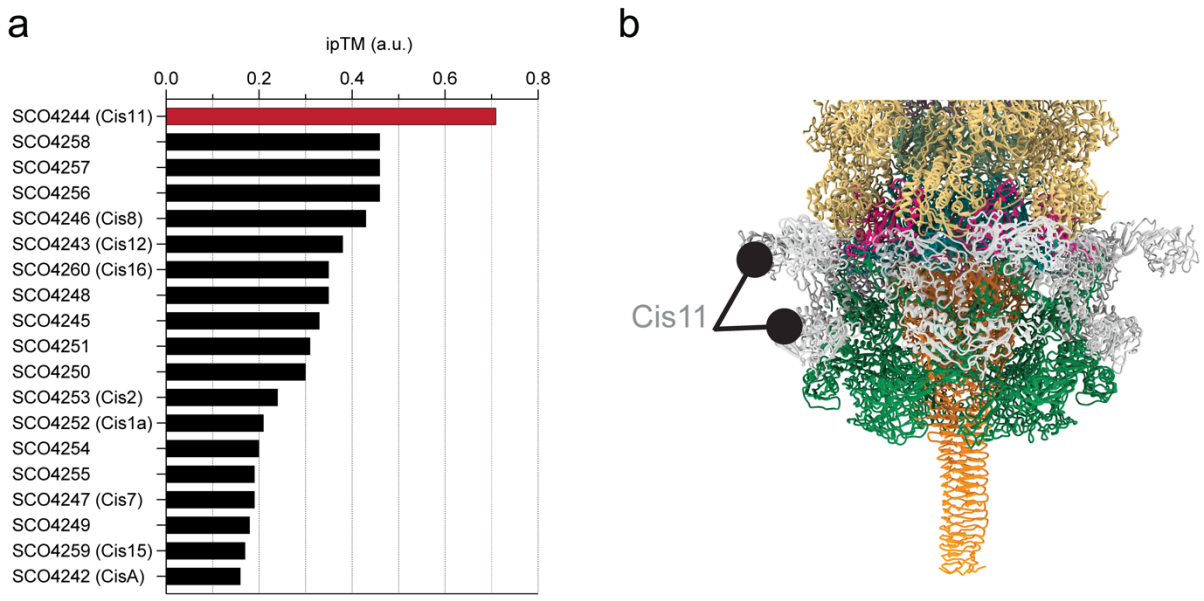

Extended Data Figure 8: *In silico* protein-protein interaction analyses of CisA and proteins of the CIS^{Sc} gene cluster.

a. An AlphaFold2-Multimer based protein-protein interaction screen between CisA and the 19 gene products of the CIS^{Sc} gene cluster suggests an interaction between CisA and the baseplate component Cis11. The likelihood of a protein-protein interaction was ranked based on the interface pTM (ipTM) confidence score, with an ipTM greater than 0.7 indicating a potential protein-protein interaction.

b. Structure of the CIS^{Sc} baseplate illustrating the peripheral and surface-exposed position of Cis11.

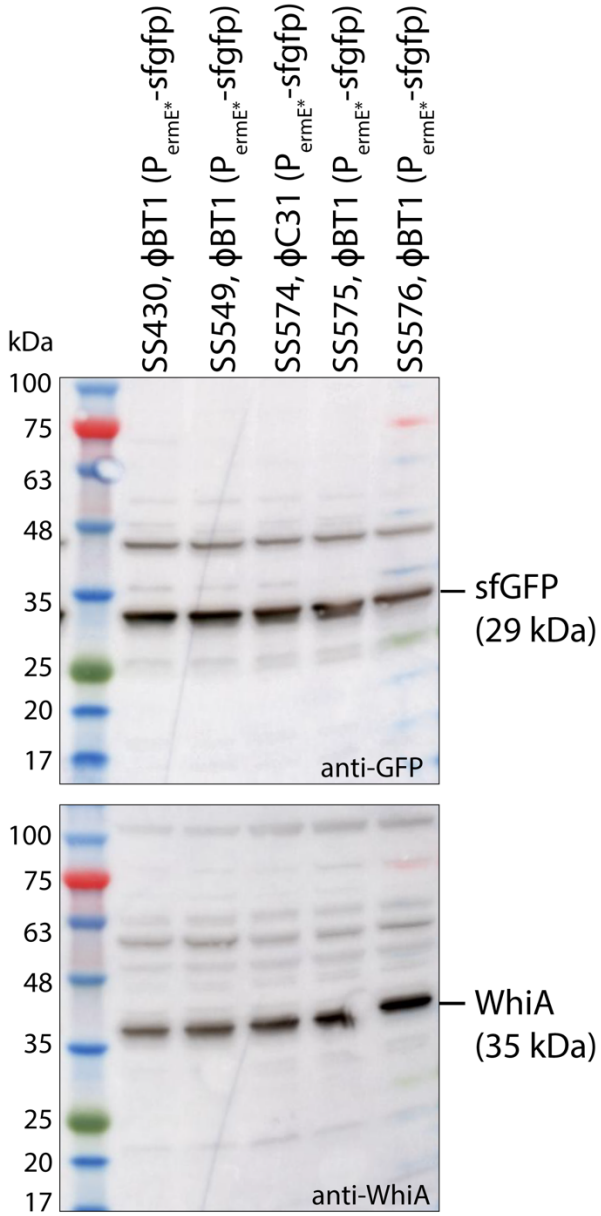

690

691 **Extended Data Figure 9: Western blot confirming similar levels of cytosolic sfGFP in**
692 **strains used for viability assays.**

693 Control experiments to verify similar protein levels of sfGFP which was expressed either from
694 the ϕC31 or the ϕBT1 phage attachment site in the *S. coelicolor* genome. Expression of *sfgfp*
695 was driven from the constitutive *ermE** promoter (P_{ermE*}). Equal amounts of total protein were
696 loaded and sfGFP levels were detected with an anti-GFP antibody. As a control, the same cell
697 lysates were also probed with an anti-WhiA antibody. Shown are representative results of
698 duplicate experiments.

699 # References

700 1. Lin, L. The expanding universe of contractile injection systems in bacteria. *Curr. Opin.*
701 *Microbiol.* **79**, 102465 (2024).
702 2. Brackmann, M., Nazarov, S., Wang, J. & Basler, M. Using Force to Punch Holes: Mechanics
703 of Contractile Nanomachines. *Trends Cell Biol.* **27**, 623–632 (2017).
704 3. Taylor, N. M. I., van Raaij, M. J. & Leiman, P. G. Contractile injection systems of
705 bacteriophages and related systems. *Mol. Microbiol.* **108**, 6–15 (2018).
706 4. Taylor, N. M. I. *et al.* Structure of the T4 baseplate and its function in triggering sheath
707 contraction. *Nature* **533**, 346–352 (2016).
708 5. Böck, D. *et al.* In situ architecture, function, and evolution of a contractile injection system.
709 *Science* **357**, 713–717 (2017).
710 6. Allsopp, L. P. & Bernal, P. Killing in the name of: T6SS structure and effector diversity.
711 *Microbiology* **169**, 001367 (2023).
712 7. Coulthurst, S. The Type VI secretion system: a versatile bacterial weapon. *Microbiol. Read.*
713 *Engl.* **165**, 503–515 (2019).
714 8. Chen, L. *et al.* Genome-wide Identification and Characterization of a Superfamily of
715 Bacterial Extracellular Contractile Injection Systems. *Cell Rep.* **29**, 511-521.e2 (2019).
716 9. Geller, A. M. *et al.* The extracellular contractile injection system is enriched in
717 environmental microbes and associates with numerous toxins. *Nat. Commun.* **12**, 3743
718 (2021).
719 10. Basler, M., Pilhofer, M., Henderson, G. P., Jensen, G. J. & Mekalanos, J. J. Type VI
720 secretion requires a dynamic contractile phage tail-like structure. *Nature* **483**, 182–186
721 (2012).
722 11. Durand, E. *et al.* Biogenesis and structure of a type VI secretion membrane core complex.
723 *Nature* **523**, 555–560 (2015).

12. Zachs, T. *et al.* Archaeal type six secretion system mediates contact-dependent antagonism. 2024.04.11.588991 Preprint at https://doi.org/10.1101/2024.04.11.588991 (2024).

13. Xu, J. *et al.* Identification and structure of an extracellular contractile injection system from the marine bacterium Algoriphagus machipongonensis. *Nat. Microbiol.* **7**, 397–410 (2022).

14. Shikuma, N. J. *et al.* Marine tubeworm metamorphosis induced by arrays of bacterial phage tail-like structures. *Science* **343**, 529–533 (2014).

15. Hurst, M. R. H., Beard, S. S., Jackson, T. A. & Jones, S. M. Isolation and characterization of the Serratia entomophila antifeeding prophage. *FEMS Microbiol. Lett.* **270**, 42–48 (2007).

16. Jiang, F. *et al.* Cryo-EM Structure and Assembly of an Extracellular Contractile Injection System. *Cell* **177**, 370-383.e15 (2019).

17. Weiss, G. L. *et al.* Structure of a thylakoid-anchored contractile injection system in multicellular cyanobacteria. *Nat. Microbiol.* **7**, 386–396 (2022).

18. Casu, B., Sallmen, J. W., Schlimpert, S. & Pilhofer, M. Cytoplasmic contractile injection systems mediate cell death in Streptomyces. *Nat. Microbiol.* **8**, 711–726 (2023).

19. Vladimirov, M., Zhang, R. X., Mak, S., Nodwell, J. R. & Davidson, A. R. A contractile injection system is required for developmentally regulated cell death in Streptomyces coelicolor. *Nat. Commun.* **14**, 1469 (2023).

20. Nagakubo, T. *et al.* Phage tail-like nanostructures affect microbial interactions between Streptomyces and fungi. *Sci. Rep.* **11**, 20116 (2021).

21. Nagakubo, T. *et al.* Intracellular Phage Tail-Like Nanostructures Affect Susceptibility of Streptomyces lividans to Osmotic Stress. *mSphere* **8**, e00114-23 (2023).

22. Nagakubo, T., Nishiyama, T., Yamamoto, T., Nomura, N. & Toyofuku, M. Contractile injection systems facilitate sporogenic differentiation of Streptomyces davawensis through the action of a phage tapemeasure protein-related effector. *Nat. Commun.* **15**, 4442 (2024).

23. Schlimpert, S. & Elliot, M. A. The Best of Both Worlds—Streptomyces coelicolor and Streptomyces venezuelae as Model Species for Studying Antibiotic Production and Bacterial Multicellular Development. *J. Bacteriol.* **205**, e00153-23 (2023).

24. Flärdh, K. & Buttner, M. J. Streptomyces morphogenetics: dissecting differentiation in a filamentous bacterium. *Nat. Rev. Microbiol.* **7**, 36–49 (2009).

25. Desfosses, A. *et al.* Atomic structures of an entire contractile injection system in both the extended and contracted states. *Nat. Microbiol.* **4**, 1885–1894 (2019).

26. Ge, P. *et al.* Action of a minimal contractile bactericidal nanomachine. *Nature* **580**, 658–662 (2020).

27. Alexeyev, M. F. & Winkler, H. H. Membrane topology of the Rickettsia prowazekii ATP/ADP translocase revealed by novel dual pho-lac reporters 1 1Edited by G. von Heijne. *J. Mol. Biol.* **285**, 1503–1513 (1999).

28. Ramos-León, F. *et al.* A conserved cell division protein directly regulates FtsZ dynamics in filamentous and unicellular actinobacteria. *eLife* **10**, e63387 (2021).

29. Bibb, M. J., Domonkos, A., Chandra, G. & Buttner, M. J. Expression of the chaplin and rodlin hydrophobic sheath proteins in Streptomyces venezuelae is controlled by σ(BldN) and a cognate anti-sigma factor, RsbN. *Mol. Microbiol.* **84**, 1033–1049 (2012).

30. Malpartida, F. & Hopwood, D. A. Molecular cloning of the whole biosynthetic pathway of a Streptomyces antibiotic and its expression in a heterologous host. *Nature* **309**, 462–464 (1984).

31. Tsao, S. W., Rudd, B. A., He, X. G., Chang, C. J. & Floss, H. G. Identification of a red pigment from Streptomyces coelicolor A3(2) as a mixture of prodigiosin derivatives. *J. Antibiot. (Tokyo)* **38**, 128–131 (1985).

32. Rapisarda, C. *et al.* In situ and high-resolution cryo-EM structure of a bacterial type VI secretion system membrane complex. *EMBO J.* **38**, e100886 (2019).

773 33. Lien, Y.-W. *et al.* Mechanism of bacterial predation via ixotrophy. 2024.01.29.577165
774 Preprint at https://doi.org/10.1101/2024.01.29.577165 (2024).
775 34. Bongiovanni, T. R. *et al.* Assembly of a unique membrane complex in type VI secretion
776 systems of Bacteroidota. *Nat. Commun.* **15**, 429 (2024).
777 35. Ouyang, R., Ongenae, V., Muok, A., Claessen, D. & Briegel, A. Phage fibers and spikes:
778 a nanoscale Swiss army knife for host infection. *Curr. Opin. Microbiol.* **77**, 102429 (2024).
779 36. Weiss, G. L. *et al.* Structure of a thylakoid-anchored contractile injection system in
780 multicellular cyanobacteria. *Nat. Microbiol.* **7**, 386–396 (2022).
781 37. T. Kieser M. J. Bibb M. J. Buttner K. F. Chater and D. A. Hopwood. *Practical Streptomyces*
782 *Genetics*. (John Innes Foundation, 2000).
783 38. Gust, B., Challis, G. L., Fowler, K., Kieser, T. & Chater, K. F. PCR-targeted Streptomyces
784 gene replacement identifies a protein domain needed for biosynthesis of the sesquiterpene
785 soil odor geosmin. *Proc. Natl. Acad. Sci. U. S. A.* **100**, 1541–1546 (2003).
786 39. Gust, B. *et al.* Lambda red-mediated genetic manipulation of antibiotic-producing
787 Streptomyces. *Adv. Appl. Microbiol.* **54**, 107–128 (2004).
788 40. Ohi, M., Li, Y., Cheng, Y. & Walz, T. Negative Staining and Image Classification -
789 Powerful Tools in Modern Electron Microscopy. *Biol. Proced. Online* **6**, 23–34 (2004).
790 41. Bush, M. J., Bibb, M. J., Chandra, G., Findlay, K. C. & Buttner, M. J. Genes Required for
791 Aerial Growth, Cell Division, and Chromosome Segregation Are Targets of WhiA before
792 Sporulation in Streptomyces venezuelae. *mBio* **4**, e00684-13 (2013).
793 42. Gallego, J. J., Severi, E., Chandra, G. & Palmer, T. Identification of novel tail--anchored
794 membrane proteins integrated by the bacterial twin--arginine translocase.
795 43. Zheng, S. Q. *et al.* MotionCor2: anisotropic correction of beam-induced motion for
796 improved cryo-electron microscopy. *Nat. Methods* **14**, 331–332 (2017).

44. Afanasyev, P. *et al.* A posteriori correction of camera characteristics from large image data sets. *Sci. Rep.* **5**, 10317 (2015).

45. P. Afanasyev. CryoEM tools. https://github.com/afanasyevp/cryoem_tools (2023).

46. Punjani, A., Rubinstein, J. L., Fleet, D. J. & Brubaker, M. A. cryoSPARC: algorithms for rapid unsupervised cryo-EM structure determination. *Nat. Methods* **14**, 290–296 (2017).

47. Wagner, T. *et al.* SPHIRE-crYOLO is a fast and accurate fully automated particle picker for cryo-EM. *Commun. Biol.* **2**, 1–13 (2019).

48. Scheres, S. H. W. RELION: implementation of a Bayesian approach to cryo-EM structure determination. *J. Struct. Biol.* **180**, 519–530 (2012).

49. Weiss, G. L., Medeiros, J. M. & Pilhofer, M. In Situ Imaging of Bacterial Secretion Systems by Electron Cryotomography. *Methods Mol. Biol. Clifton NJ* **1615**, 353–375 (2017).

50. Mastronarde, D. N. Automated electron microscope tomography using robust prediction of specimen movements. *J. Struct. Biol.* **152**, 36–51 (2005).

51. Kremer, J. R., Mastronarde, D. N. & McIntosh, J. R. Computer visualization of three-dimensional image data using IMOD. *J. Struct. Biol.* **116**, 71–76 (1996).

52. Tegunov, D. & Cramer, P. Real-time cryo-electron microscopy data preprocessing with Warp. *Nat. Methods* **16**, 1146–1152 (2019).

53. Emsley, P., Lohkamp, B., Scott, W. G. & Cowtan, K. Features and development of Coot. *Acta Crystallogr. D Biol. Crystallogr.* **66**, 486–501 (2010).

54. Song, Y. *et al.* High-resolution comparative modeling with RosettaCM. *Struct. Lond. Engl. 1993* **21**, 1735–1742 (2013).

55. Adams, P. D. *et al.* PHENIX: a comprehensive Python-based system for macromolecular structure solution. *Acta Crystallogr. D Biol. Crystallogr.* **66**, 213–221 (2010).

56. Schindelin, J. *et al.* Fiji - an Open Source platform for biological image analysis. *Nat. Methods* **9**, 10.1038/nmeth.2019 (2012).

822 57. Jumper, J. *et al.* Highly accurate protein structure prediction with AlphaFold. *Nature* **596**,
823 583–589 (2021).
824 58. Ef, P. *et al.* UCSF Chimera--a visualization system for exploratory research and analysis.
825 *J. Comput. Chem.* **25**, (2004).
826 59. Goddard, T. D. *et al.* UCSF ChimeraX: Meeting modern challenges in visualization and
827 analysis. *Protein Sci. Publ. Protein Soc.* **27**, 14–25 (2018).
828 60. Mirdita, M. *et al.* ColabFold: making protein folding accessible to all. *Nat. Methods* **19**,
829 679–682 (2022).
830 61. McLean, T. C. LazyAF, a pipeline for accessible medium-scale *in silico* prediction of
831 protein-protein interactions. Preprint at https://doi.org/10.1101/2024.01.29.577767 (2024).
832 62. O'Reilly, F. J. *et al.* Protein complexes in cells by AI -assisted structural proteomics. *Mol.*
833 *Syst. Biol.* **19**, e11544 (2023).
834 63. Zhang, Y., Wang, L., Zhang, S., Yang, H. & Tan, H. hmgA, transcriptionally activated by
835 HpdA, influences the biosynthesis of actinorhodin in Streptomyces coelicolor. *FEMS*
836 *Microbiol. Lett.* **280**, 219–225 (2008).
837

Table EV1. Cryo-EM data statistical analysis

	Cap	Baseplate_C6 (overall)	Baseplate_C3
Data collection and processing			
Nominal magnification		81,000	
Voltage (kV)		300	
Electron exposure (e^-/Å)		~60 (K3 camera)	
Defocus range (μm)		1.0 - 3.0	
Pixel size (Å/pixel)		1.065	
Symmetry imposed	C6	C6	C3
Initial particles (No.)	36,569	43,087	36,569
Final particles (No.)	19,218	22,920	18,124
Map resolution (Å)	3.4	3.5	3.8
FSC threshold		0.143	
Refinement			
Model composition			
Atoms	33006 (Hydrogens: 243)	141138 (Hydrogens: 0)	14343 (Hydrogens: 0)
Protein residues	4266	18408	1923
Chains	18	60	3
R.M.S deviations			
Bond length (Å)	0.003	0.007	0.005
Bond angles (˚)	0.558	0.839	0.768
Validation			
MolProbity score	1.51	2.22	1.91
Clashscore	5.77	14.01	7.86
Rotamer outlier (%)	0.03	0.04	0
Ramachandran plot			
Favored (%)	96.81	89.51	92.18
Allowed (%)	3.19	10.46	7.82
Outlier (%)	0	0.44	0
Masked CC	0.77	0.79	0.77

Table EV2. Proteins detected by mass spectrometry in samples of purified CIS^{Sc} after crude sheath preparation from a *S. coelicolor* non-contractile CIS^{Sc} mutant without exogeneous stress and following nisin stress.

Protein ID	CIS ID	*S. coelicolor* CIS-N5	
		Without exogeneous stress	Upon nisin stress
SCO4242	CisA	-	5% coverage / 2 total unique peptide
SCO4243	Cis12	6% coverage / 1 total unique peptide	5% coverage / 1 total unique peptide
SCO4244	Cis11	13% coverage / 6 total unique peptide	4% coverage / 2 total unique peptide
SCO4245	Cis9	21% coverage / 2 total unique peptide	20% coverage / 2 total unique peptide
SCO4246	Cis8	18% coverage / 10 total unique peptide	13% coverage / 7 total unique peptide
SCO4247	Cis7	5% coverage / 1 total unique peptide	4% coverage / 1 total unique peptide
SCO4248	Cis1b	22% coverage / 2 total unique peptide	20% coverage / 2 total unique peptide
SCO4249	-	5% coverage / 1 total unique peptide	4% coverage / 1 total unique peptide
SCO4252	Cis1a	26% coverage / 4 total unique peptide	19% coverage / 3 total unique peptide
SCO4253	Cis2	23% coverage / 9 total unique peptide	30% coverage / 14 total unique peptide
SCO4254	-	10% coverage / 6 total unique peptide	10% coverage / 6 total unique peptide
SCO4256	-	17% coverage / 7 total unique peptide	22% coverage / 9 total unique peptide
SCO4257	-	-	-
SCO4258	-	-	-
SCO4259	Cis15	-	-
SCO4260	Cis16	20% coverage / 4 total unique peptide	17% coverage / 3 total unique peptide

Table EV3: Strains and plasmids used in this study

Strain	Description	Construction	Source
Escherichia coli strains			
TOP10	*F⁻ mcrA Δ(mrr-hsdRMS-mcrBC) Φ80lacZΔM15 ΔlacX74 recA1 araD139 Δ(ara leu) 7697 galU galK rpsL (StrR) endA1 nupG*	Cloning	Lab strain
ET12567/pUZ8002	*F⁻ dam13::Tn9 dcm6 hsdM hsdR recF143:: Tn10 galK2 galT22 ara-14 lacY1 xyl-5 leuB6 thi-1 tonA31 rpsL hisG4 tsx-78 mtl-1 glnV44*	ET12567 with helper plasmid pUZ8002	[1]
BW25113/pIJ790	*Δ(araD-araB)567 ΔlacZ4787(::rrnB-4) lacIp-4000(lacIQ), λ−rpoS369(Am) rph-1 Δ(rhaD-rhaB)568 hsdR514*	BW25113 containing λ RED recombination plasmid pIJ790	[2]
NEB5-alpha	*fhuA2Δ(argF-lacZ)U169 phoA glnV44 Φ80 Δ(lacZ)M15 gyrA96 recA1 relA1 endA1 thi-1 hsdR17*	Cloning	NEB
Rosetta (DE3)	*F⁻ ompT hsdSB(rB⁻ mB-) gal dcm (DE3) pRARE (Cam^R)*	Host strain for protein overexpression	Merck
TG1	*supE thi-1 Δ(lac-proAB) Δ(mcrB-hsdSM)5 (rK-mK) / F´ traD36 proAB lacIqZΔM15*	Topology Experiment	Lab Strain
Streptomyces coelicolor strains			
S. coelicolor M145	Wild type (SCP1-, SCP2-)		[3]
SS387	Δ*SCO4253-51::apr, apr^R*		[4]

SS393	Δ*SCO4253-51::apr attB ϕBT1 (SCO4253-N5-SCO4252-51), hyg*^{R}		[4]
SS430	WT *ϕBT1 (PermE*-sfgfp)*		[4]
SS539	Δ*SCO4242::apr, apr*^{R}	chromosomal *SCO4242 (cisA)* locus deleted using pSS684	This study
SS549	Δ*SCO4242::apr ϕBT1 (PermE*-sfgfp)*	pSS150 integrated at ΦBT1 attachment site of SS539	This study
SS557	Δ*SCO4242 ϕBT1(PermE*-SCO4242-3xFLAG) hyg*^{R}*, apr*^{R}	pSS735 integrated at ϕBT1 attachment site of SS539	This study
SS574	WT *ϕC31 (PermE*-sfgfp), apr*^{R}*, thio*^{R}	pSS758 integrated at ϕC31 attachment site of WT	This study
SS575	Δ*SCO4242::apr ϕC31 (PermE*-sfGFP) apr*^{R}*, thio*^{R}	pSS758 integrated at ϕC31 attachment site of SS539	This study
SS576	Δ*SCO4242:apr ϕBT1(PermE*-SCO4242-3xFLAG) ϕC31 (PermE*-sfGFP) apr*^{R}*, thio*^{R}*, hyg*^{R}	pSS758 integrated at ϕC31 attachment site of SS557	This study
JS65	Δ*SCO4242:apr ϕBT1(PermE*-) hyg*^{R}*, apr*^{R}	pIJ10257 integrated at ϕBT1 attachment site of SS387	This Study
JS69	Δ*SCO4242:apr ϕBT1(PermE*-SCO4242-mcherry) hyg*^{R}*, apr*^{R}	pSS705 integrated at ϕBT1 attachment site of SS387	This study
Cosmid and Plasmids			
StD8A	Cosmid vector containing coding sequence for *SCO4242* km^R, carb^R		http://strepdb.streptomyces.org.uk
pIJ773	pBluescript KS (+) containing the apramycin resistance gene *apr* and *oriT* of plasmid RP4,		[5]

	flanked by FRT sites (Apr^R). Used as template for the amplification of the *apr-oriT* cassette for 'REDIRECT' PCR targeting, apr^R		
pIJ10257	Cloning vector for the conjugal transfer of DNA (under control of the *ermE** constitutive promoter). Integrates at the *ΦBT1* attachment site, hyg^R		[6]
pET21b	Plasmid for overexpression of proteins in *E. coli*, *carb^R*		Lab stock
pKF351	Derivative of pKF280, integrates at the *ΦC31* attachment site, apr^R		[7]
pSS150	pIJ10257 carrying *PermE*-sfgfp*, hyg^R		[4]
pSS684	Mutated cosmid StD8A for REDIRECT containing *ΔSCO4242::apr, km^R, carb^R, apr^R*	The *SCO4242* coding sequence on the cosmid vector StD8A was replaced by an *oriT*-containing apramycin resistance cassette, which amplified from pIJ773 using primer 1676/1677	This study
pSS88	pIJ10257 carrying *mcherry*, *hyg^R*	*Streptomyces* Codon-optimised *mcherry* was inserted between the NdeI-XhoI site of pIJ10257.	This study
pSS705	*PermE*-SCO4242-mcherry, hyg^R*	*SCO4242* coding sequence amplified with primer 1731/1732 and assembled with pSS88 cut with NdeI-XhoI.	This study
pSS734	*PermE*-SCO4242- TEV-sfgfp, hyg^R*	A "GGS-TEV" amino acid sequence was added upstream of *sfgfp* from pSS150 by PCR using	This study

		primer 1800/1801. The PCR product was cut with XhoI-AvrI and inserted into pSS705 cut with the same enzymes.	
pSS735	*PermE*-SCO4242-3xFLAG, hyg*^{R}	*PermE*-SCO4242* fragment was isolated from pSS705 by restriction digestion with KpnI-XhoI and ligated with pIJ10257 cut with KpnI-XhoI.	This study
pSS758	pKF351 carrying *PermE*-sfgfp, apr*^{R}*, thio*^{R}	*sfgfp* amplified from pSS150 with primer 1851/1852 and assembled into pKF351 cut with BamHI-KpnI.	This study
Plasmid used to test membrane topology			
pKTop	Plasmid encoding a dual *pho-lac* reporter, km^R		[8]
pFRL1	Plasmid encoding the known *Streptomyces* cytoplasmic protein, SepH, in the dual *pho-lac* reporter, *km*^{R}		Felix Ramos-Leon (unpublished)
pFRL5	Plasmid encoding the *Streptomyces* membrane protein, RsbN, in the dual *pho-lac* reporter, *km*^{R}		Felix Ramos-Leon (unpublished)
pJUK131	pKTop carrying *SCO4242, km*^{R}	Codon optimized *SCO4242* amplified with primers JS111/JS112 from pJUK123 digested and inserted into *HinDIII*/*Kpn*I digested pKTop	This study
pJUK132	pKTop carrying *SCO4242* (1-310aa), *km*^{R}	Codon optimized *SCO4242* containing only codons for aa 1-310 amplified with primers JS111/JS113 from pJUK123 digested and inserted into *HinDIII*/*Kpn*I digested pKTop	This study
pJUK145	pKTop carrying *SCO4242* (1-285aa), *km*^{R}	Codon optimized *SCO4242* containing only codons for aa 1-285 amplified with primers JS111/JS114 from pJUK123 digested and inserted into HinDIII/KpnI digested pKTop	This study

pJUK146	pKTop carrying *SCO4242* (Δ295-305aa), *km*^{R}	Codon optimized SCO4242 omitting codons for aa 295-310 amplified with primers JS111/JS112 from pJUK133 digested and inserted into HinDIII/KpnI digested pKTop	This study

Table EV4: Oligonucleotides used in this study.

Name	Sequence (5'→3')
1676	GGAGAGATGACCACGCAGAACTGCGCCGAGTGCGGAACCATTCCGGGGATCCGTCGACC
1677	CGGCCCGGGTCAGGAGGAGCGGTTGGCGCTGGACGGGCCTGTAGGCTGGAGCTGCTTC
1691	ATATTCTAGAGATGACCACGCAGAACTGCGCC
1692	ATATGGTACCTCAGGAGGAGCGGTTGGCGC
1693	ATATAAGCTTGATGCCCCTGCCCTCTCCCAAC
1694	ATATGGTACCCGCGCGCTGTCCCCGATCACG
1731	TGGTAGGATCGTCTAGAACAGGAGGCCCCATATGACCACGCAGAACTGCGCC
1732	ATGTTGTCCTCCTCGCCCTTGGAGACCATCTCGAGGGAGGAGCGGTTGGCGCT
1767	AGCTGTTTCCTGTGTGAAATTGTTATCC
1800	ATATACTCGAGGGTGGCTCCGAAAACCTGTACTTCCAATCCATGTCCAAGGGCGAGGAGC
1801	AATTAACCTAGGTCACTTGTACAGCTCGTCCATGCC
1851	AAGTCGTGCTGCTTCATGTGGTCGGGGTACCCGACCCGAGCACGCG
1852	ATTACTGGACCGGATGAATTCACTTGGATCCGTTAATTAATCACTCGAGCTCCGGGCCCG
1930	CCAAGCTTGCATGCCTGCAGG
1931	TCACACAGGAAACAGCTATGACCACGCAGAACTGCGCC
1932	GGCATGCAAGCTTGGGATGCGGTCGAAGACGCGGC
1933	CCAAGCTTGCATGCCTGCAGG
1934	GGCATGCAAGCTTGGGATGCGGTCGAAGACGCGGC
JS105	CCTCCGCGAATCGGTCGTCTCTCGAGGGTGGCTCCGAAAACCT
JS106	GCGCAATTTTGGGTCGTCATATGTATATCTCCTTCTTAAAGTTAAACAAAATTATTTCTAGAGGGGAA
JS107	TTTAAGAAGGAGATATACATATGACGACCCAAAATTGCGCCGAATGT
JS108	TTTTCGGAGCCACCCTCGAGAGACGACCGATT
JS111	CATTAGAAGCTTTATGACGACCCAAAATTGCGCCG
JS112	CATTAGGGTACCGACGACCGATTCGCGGAGG
JS113	CATTAGGGTACCTGAACCCCGTCGGGAATATA
JS114	CATTAGGGTACCCCGATTCGATCGAAAACACGACGC

References:

1. Paget, M. S. B., Chamberlin, L., Atrih, A., Foster, S. J. & Buttner, M. J. Evidence that the Extracytoplasmic Function Sigma Factor çE Is Required for Normal Cell Wall Structure in Streptomyces coelicolor A3(2). *J. Bacteriol.* **181**, 204–211 (1999).
2. Datsenko, K. A. & Wanner, B. L. One-step inactivation of chromosomal genes in Escherichia coli K-12 using PCR products. *Proc. Natl. Acad. Sci.* **97**, 6640–6645 (2000).
3. T. Kieser M. J. Bibb M. J. Buttner K. F. Chater and D. A. Hopwood. *Practical Streptomyces Genetics*. (John Innes Foundation, Norwich, 2000).
4. Casu, B., Sallmen, J. W., Schlimpert, S. & Pilhofer, M. Cytoplasmic contractile injection systems mediate cell death in Streptomyces. *Nat. Microbiol.* **8**, 711–726 (2023).
5. Gust, B., Challis, G. L., Fowler, K., Kieser, T. & Chater, K. F. PCR-targeted Streptomyces gene replacement identifies a protein domain needed for biosynthesis of the sesquiterpene soil odor geosmin. *Proc. Natl. Acad. Sci. U. S. A.* **100**, 1541–1546 (2003).
6. Hong, H.-J., Hutchings, M. I., Hill, L. M. & Buttner, M. J. The role of the novel Fem protein VanK in vancomycin resistance in Streptomyces coelicolor. *J. Biol. Chem.* **280**, 13055–13061 (2005).
7. Schlimpert, S. *et al.* Two dynamin-like proteins stabilize FtsZ rings during Streptomyces sporulation. *Proc. Natl. Acad. Sci.* **114**, E6176–E6183 (2017).
8. Karimova, G., Robichon, C. & Ladant, D. Characterization of YmgF, a 72-Residue Inner Membrane Protein That Associates with the Escherichia coli Cell Division Machinery. *J. Bacteriol.* **191**, 333–346 (2009).